$Na_v1.1$ N722D mutant causes Dravet Syndrome through loss-of-function

by

Ananya Sridhar

B.Tech. Biotechnology, Vellore Institute of Technology, 2020

Thesis Submitted in Partial Fulfillment of the
Requirements for the Degree of
Master of Science

in the
Department of Biomedical Physiology and Kinesiology
Faculty of Science

SIMON FRASER UNIVERSITY
Fall 2022

Declaration of Committee

Name:	**Ananya Sridhar**
Degree:	**Master of Science (Biomedical Physiology and Kinesiology)**
Title:	**$Na_v1.1$ N722D mutant causes Dravet Syndrome through loss-of-function**
Committee:	**Chair:** **Charles Krieger** Professor, Biomedical Physiology and Kinesiology
	Peter Ruben Supervisor Professor, Biomedical Physiology and Kinesiology
	Thomas Claydon Committee Member Professor, Biomedical Physiology and Kinesiology
	Sam Doesburg Committee Member Associate Professor, Biomedical Physiology and Kinesiology
	Sam Goodchild Examiner Principal Research Scientist Xenon Pharmaceuticals Ltd.

Abstract

Dravet Syndrome (DS) is an epileptic encephalopathy that affects 1 in 30,000 children globally. Characterized by seizure onset after relatively normal early development, 80% of DS cases are monogenic in origin and associated with mutations in the Sodium Channel Type 1 Alpha (*SCN1A*) gene. *SCN1A* encodes the voltage-gated sodium channel, $Na_v1.1$, that plays a vital role in action potential generation and propagation in central nervous system neurons. Due to heterogeneity in the causative variant and observed phenotype, there is a need to characterize each novel mutation associated with DS. I characterized the DS-associated mutant N722D using patch-clamp, immunocytochemistry, and computational modelling. N722D does not significantly alter channel activation or inactivation. However, N722D decreases $Na_v1.1$ current density and membrane expression. Supported by information obtained from action potential modelling, I suggest that N722D causes DS due to loss-of-function primarily by altering the trafficking of $Na_v1.1$ to the plasma membrane in neurons.

Keywords: Epilepsy; Dravet Syndrome; Sodium channel; $Na_v1.1$; Electrophysiology

Acknowledgements

I would like to begin by expressing a grateful thank you to my supervisor, Dr. Peter Ruben, for being an absolute unicorn of a supervisor. No words are enough to express my gratitude for all the encouragement, support, infinite amounts of patience and kind words you've provided no matter what the situation. I also could not have undertaken this journey without my thesis supervisory committee, Dr. Thomas Claydon and Dr. Sam Doesburg, who generously shared their time, knowledge, and expertise and helped bring this thesis into existence.

A great deal of gratitude is due to my mentor, Dr. Dana Page for always going above and beyond what duty calls for. Dana, I've learnt so much from you over the course of these two years that I would be remiss to not say thank you. For the teaching, the editing, the moral (and sometimes emotional) support, and most importantly, the friendship. I would also like to take this opportunity to thank Dr. Mohamed Fouda and all the members of the Ruben Lab and MCPG for their valuable inputs and help, without which the progress of this work would have been dawdling.

And my biggest thanks to my friends and family for all the love, immeasurable support, and encouragement you have shown me through these two years. You guys are the people that kept me inspired and set an example everyday of what true passion and love for your work looks like. I promise my zombie writing phase is almost done, thank you for making sure I was fed and hydrated so I could at least behave like a semi-functional human for the past month.

Table of Contents

List of Tables

List of Figures

List of Abbreviations

AED	Anti-Epileptic Drugs
AKAP	A-Kinase Anchoring Proteins
ASD	Autism Spectrum Disorders
BCA	Bicinchoninic acid
BFP	Blue Fluorescent Protein
BSA	Bovine Serum Albumin
Ca^{2+}	Calcium ions
$CaCl_2$	Calcium Chloride
CFTR	Cystic Fibrosis Transmembrane Conductance Regulator
CNS	Central Nervous System
CsCl	Caesium Chloride
CsF	Caesium Fluoride
CsOH	Caesium Hydroxide
DMEM	Dulbecco's Modified Eagle's Medium
DS	Dravet Syndrome
DTT	Dithiothreitol
eGFP	Enhanced green fluorescent protein
E_{Na}	Equilibrium Potential
ER	Endoplasmic Reticulum
FBS	Foetal Bovine Serum
FI	Fast Inactivation
GABA	Gamma-aminobutyric Acid
$GEFS^{+}$	Generalized Epilepsy Febrile Seizures Plus
G_{Na}	Sodium channel Conductance
HEK293T	Human Embryonic Kidney Cells
HEPA	High efficiency particulate air
IGEPAL	Octylphenoxypolyethoxyethanol
I_{Na}	Sodium Current
I_{NaP}	Persistent Current

I_{SS}	Steady state current
K^+	Potassium ions
KCl	Potassium Chloride
KO	Knock out
$MgCl_2$	Magnesium Chloride
Na^+	Sodium ions
Na_vs	Voltage gated sodium channels
PBS	Phosphate buffered saline
PKA	Protein Kinase A
PKC	Protein Kinase C
PNS	Peripheral Nervous System
PV^+	Parvalbumin positive
SCN1A	Sodium Channel Type 1 Alpha
SDS-PAGE	Sodium Dodecyl Sulfate Polyacrylamide Gel Electrophoresis
SEM	Standard Error of Mean
SMEI	Severe Myoclonic Epilepsy of Infancy
SST^+	Somatostatin positive
V_m	Test pulse membrane potential
VSD	Voltage Sensing Domain
WT	Wild Type

Chapter 1. Introduction

1.1. Neuronal excitability and the discovery of sodium channels

In the late 1700s, an Italian scientist, Luigi Galvani used a dead frog to study the ability of the nervous system to conduct electricity. The main aim of conducting this experiment was to undeniably verify the “neuroelectric theory” and its implications for the human body. The neuroelectric theory postulated that an external source of artificial electricity was the cause for the excitation of nervous and muscular tissue and caused them to contract. However, what Galvani found was not in accordance with this theory. Instead, what he found was that nerves and muscles contracted when being touched using a conductive material whereas no change occurred when an insulative material was used. Galvani was the first scientist to come up with the theory of there being electrical conduction in the nervous system, that he coined “animal electricity”[1]. Additionally, he hypothesized about the strength of the stimulus required to elicit a proportional response from these systems. He found that there was no direct proportionality that could explain the contraction observed. There was, however, a requirement that the stimulus needed to surpass a certain threshold value in order to elicit any response from the nerve and muscle fibres[2]. The work of Luigi Galvani was the foundation of what we call electrophysiology today.

It was only in the 20th century that the exact mechanism of neuronal conduction was understood. A series of publications by Hodgkin and Huxley brought to light the crucial role played by sodium channels and the contribution of inward sodium (Na^+) current to the generation and propagation of action potentials in the giant squid axon[3–6]. This study revealed the importance of large transmembrane channels that rely on changes in the membrane electrical potential to open and close while selectively allowing the specific influx of Na^+ ions. These channels serve as the gatekeepers of electrical excitability in excitable cells and can have disastrous consequences when their gating properties are altered (either enhanced or reduced).

1.2. An introduction to sodium channels

In the mammalian central nervous system, voltage-gated sodium channels (Na_vs) initiate and propagate action potentials when they receive excitatory inputs that are greater than the threshold membrane depolarization potential. Voltage-gated sodium channels comprise a 260 kDa α-subunit[7–10] and one or more supplementary 30-40 kDa β-subunits.[11–14] The sodium channel α subunit consists of four domains (DI-IV), which are structurally homologous to one another and each contains six α-helical transmembrane segments (S1- S6)[15,16]. The voltage-sensor in each of the domains is located in the S1-S4 segments. S4 contains positively charged amino-acid residues in every third position. The narrow, ion-selectivity filter motif is made up of four glutamate residues at the extracellular end of the pore. It is formed by the embedding of a re-entrant loop between helices S5 and S6 within the transmembrane region of the channel and allows the passage of only Na^+ ions, not K^+ or Ca^{2+} ions, imparting the characteristic selectivity to the channel[17]. The S6 segments from each domain together form the wider intracellular end of the pore.[18] Small extracellular and intracellular loops connect the transmembrane segments, with the largest ones connecting the S5 or S6 segments to the membrane re-entrant loop[19]. Larger intracellular loops link the four homologous domains. The intracellular loop connecting homologous domains I and II (loop I-II) contains many functionally relevant phosphorylation sites in most isoforms. Other intracellular regions contain additional targets for isoform-specific phosphorylation and protein-protein interactions.[20,21]

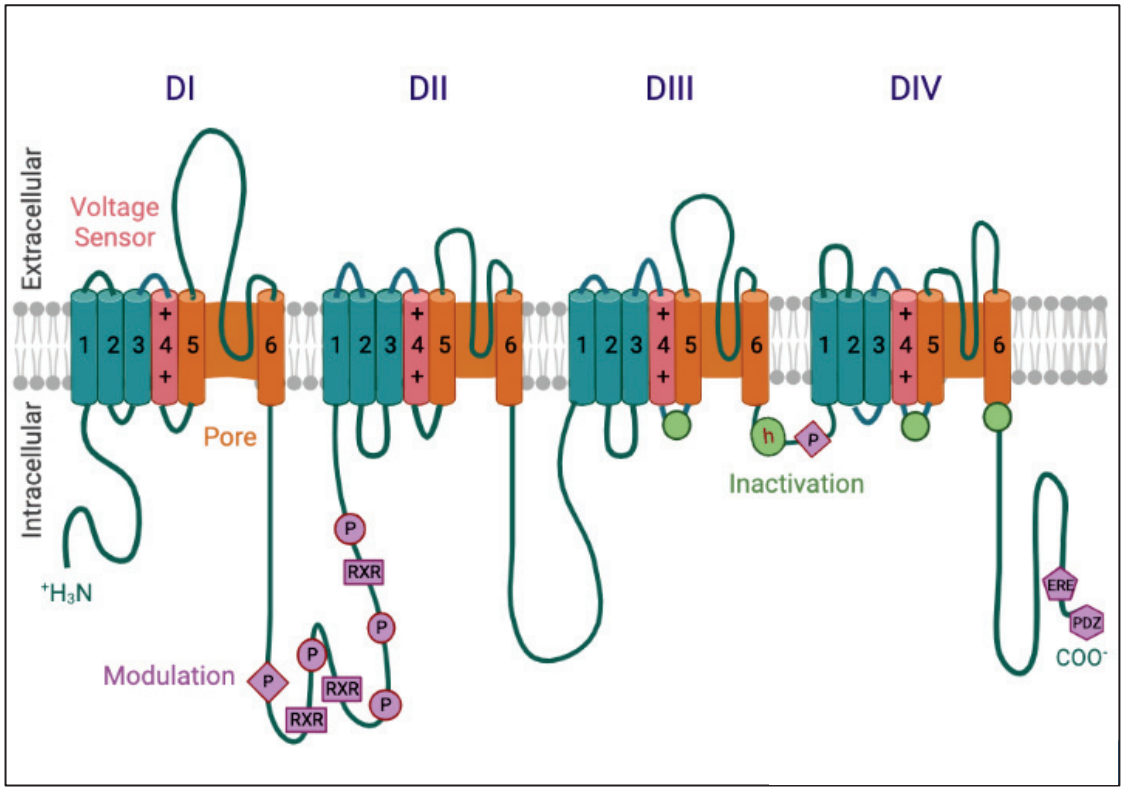

Figure 1: Structure of voltage gated sodium channels
The primary structure of voltage gated sodium channels is depicted in the form of transmembrane folding diagrams. Cylinders represent α-helical segments. Bold lines represent the polypeptide chains linking each segment and domain. Orange, pore-lining segments; pink, S4 voltage sensors; h in green circle, inactivation particle in the inactivation gate loop; green circles, sites that form the inactivation gate receptor; interacting protein sites shown in purple, P represents phosphorylation sites by PKA (circles) and PKC (diamonds); ERE is site for binding of ER exporting motif, RXR is the site for ER retention motif and PDZ is the site for syntrophin modulation. Figure created on BioRender.com

1.3. Voltage-Gated Sodium Channel Gating

Na_vs exist in one of three states at any given time: resting, open, or inactive (Figure 2). In the resting (closed) and inactive state, they are impermeable to Na^+ ions, effectively preventing the passage of ions through the channel. Ion conduction is only possible when the channel is in the open (active) state. To put it simply, depolarization of the membrane leads to the transitioning of the channel from the resting state to the active state, permitting the flow of Na^+ ions along the concentration gradient. This process is called channel activation. Following activation, within a span of 1-2 milliseconds, four hydrophobic amino acid residues (IFMT), collectively known as the inactivation particle, located within the intracellular linker of DIII and DIV, bind to the S4-S5 cytoplasmic linker of DIII and DIV after undergoing a conformational change. This channel inactivation, also known as fast-inactivation (FI), blocks the ion permeating pore to halt ion conductance thereby terminating sodium influx (I_{Na})[22–26]. Recovery from fast inactivation is the process of channels returning to the resting state from the inactivated state, completing the cycle of channel gating transitions at the same time[23]. The time course of entry into and recovery from FI plays an important role in determining channel availability for subsequent action potential generation. Sodium channel FI is responsible for the absolute refractory period of an action potential and supports the propagation of action potentials in a unidirectional manner. This happens due to the unavailability of previous channels that haven't recovered from FI and hence cannot be re-excited. Most channel modulators, like venom peptides have the ability to regulate ion permeability through the channel and alter the cycle of transition between different states mentioned above[27] resulting in serious clinical consequences.

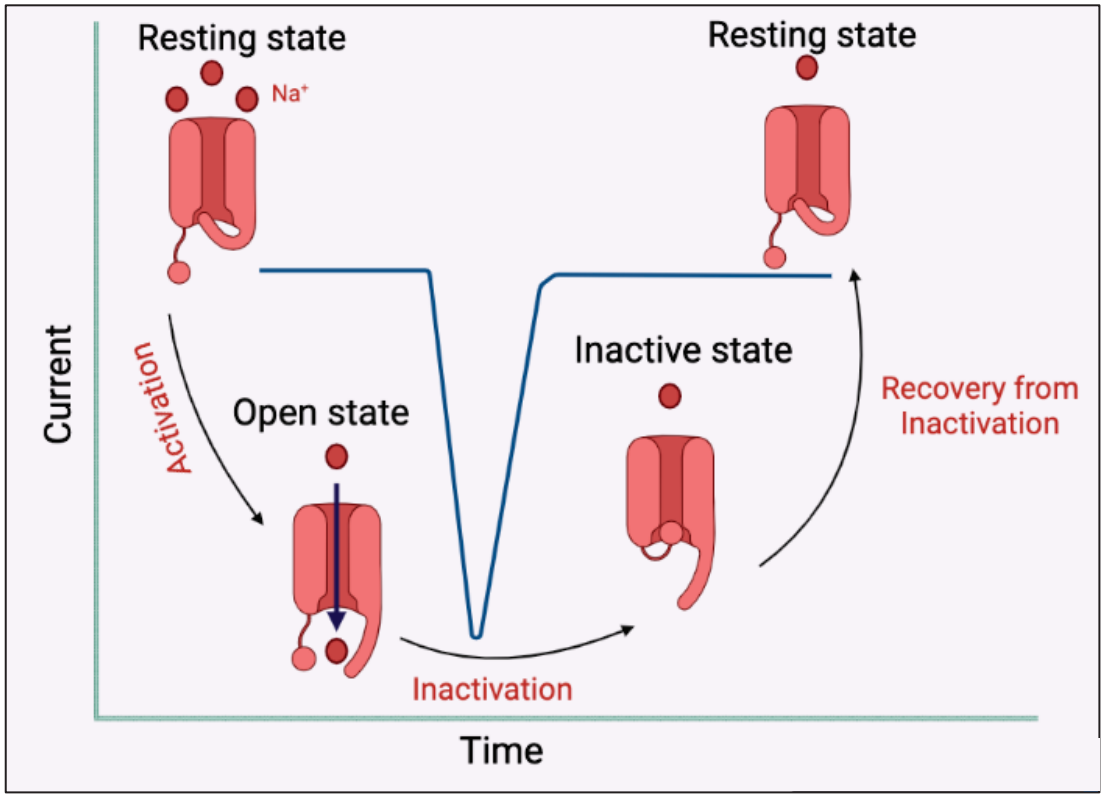

Figure 2: Gating in Na_vs is a cyclical process.
Upon depolarization, Na_v channels transition from the closed or resting to open state, which makes permeation of Na^+ ions through the pore possible. Fast inactivation then leads to obstruction of the pore by the inactivation particle, preceding the return to the closed state once membrane potential returns to resting levels. Figure created on BioRender.com.

1.4. Diversity in sodium channels

There are currently 12 different α subunits in the genome that have been functionally expressed and characterized. These have been classified into three subclasses or families. From family type 1, $Na_v1.1$, $Na_v1.2$, $Na_v1.3$, and $Na_v1.6$ are referred to as neuronal sodium channels due to their high occurrence within the central nervous and peripheral nervous systems. $Na_v1.4$ is found predominately in skeletal muscles and $Na_v1.5$ is found in cardiac muscles, embryonic, and denervated muscles. Two of these isoforms, $Na_v1.7$ and $Na_v1.8$ are expressed primarily in the peripheral nervous system. Three members from the type 2 family are also included in this list, $Na_v2.1$ and $Na_v2.3$ usually found in heart tissue, and $Na_v2.2$ (NaG) found in astrocytes. Recently, a newer isoform, $Na_v3.1$ (NaN), was cloned from dorsal root ganglion (DRG) tissue. This isoform shows less than 50% similarity to either of the other two families and

may be representative of a third (type 3) family of sodium channels[28–30]. The transmembrane portions of different isoforms within a family are highly conserved. The biggest structural difference lies in the N- and distal C-termini as well as in the first two intracellular loops connecting the homologous domains.[31] Put together, mutations in different families of sodium channels are responsible for a wide range of channelopathies including various forms of Epilepsy, Autism Spectrum Disorders (ASD), Myotonia, Migraines, Long QT Syndrome, Familial Pain syndromes, Erythromelalgia and Brugada syndrome to name a few[31,32].

1.5. $Na_V1.1$ Localization and Epilepsy

$Na_v1.1$, also known as the α type I sodium channel, is encoded by the *SCN1A* gene located on the chromosome 2q24. Found predominantly throughout various types of neurons in the central nervous system (CNS), $Na_v1.1$ is a hotspot for the occurrences of mutations and is one of the most commonly studied genes when it comes to characterizing epileptic phenotypes. $Na_v1.1$ is expressed in the somatodendritic regions of pyramidal cells and inhibitory interneurons as well as in the cell bodies and proximal side of the axon initial segments of retinal ganglion cells, dentate granule cells and cerebellar Purkinje cells[33]. It is also expressed in neurons in the spinal cord including motor neurons. Loss of $Na_v1.1$ expression in GABAergic interneurons is associated with the paradoxical global hyperexcitability caused by mutations in the $Na_v1.1$ protein[34].

Depending on the site of mutation in the channel and type of mutation, $Na_v1.1$ channelopathies lead to seizures. The range of seizure conditions, however, is a spectrum with mild familial febrile epilepsy and only a partial loss of function on one end to catastrophic epileptic disorders like Dravet Syndrome (DS) or Generalized epilepsy with Febrile Seizures Plus (GEFS+) having more serious phenotypic markers on the other[35–37]. Febrile seizures occur in less than 5% of all children under the age of six and are typically not associated with an increased risk of epilepsy in adolescence and adulthood[38]. In complete contrast to this, GEFS+, an autosomal dominant disorder causes febrile seizures that persist beyond six years of age. These are additionally associated with generalized or partial epilepsies, such as absence epilepsy, myoclonic seizures, atonic seizures, and myoclonic-astatic epilepsy[39–41].

The path to the discovery of how different mutations in $Na_v1.1$ cause epileptic phenotypes was a long and arduous journey. When the identification of the first epileptogenic mutation in *SCN1A* was characterized using an animal model, all available data suggested that $Na_v1.1$ was expressed only in glutamatergic pyramidal cells, which are excitatory in nature. Therefore, it was incredibly puzzling that loss-of-function mutations causing epilepsy, a disorder characterized by brain hyperexcitability, could lead to reduced Na^+ current and by default to reduced neuronal excitability in the brain. This inconsistency was explained by developing and studying specific genetically modified mice carrying *Scn1a* mutations.

In the first study looking at gene-targeted mice carrying *Scn1a* mutations, Yu et al.,[42] investigated the generation and pathophysiology of a complete knockout (KO) mouse model of a truncating DS mutation. Heterozygous KO (*Scn1a*$^{+/-}$ or *Scn1a*^{tm1Wac}) mice displayed seizures (including those caused by an increase in temperature) and sporadic deaths beginning at postnatal day, P21, with genetic background dependent severity. A very severe phenotype in the C57Bl/6 strain, a mild phenotype in the 129 strain, and an intermediate phenotype in the mixed C57Bl/6-129F1 strain. They observed a reduction in the Na^+ current density without any other alterations of gating properties in GABAergic interneurons, causing hypoexcitability in them, but having no effect on the firing of glutamatergic excitatory neurons. These results suggested that the decreased excitability of GABAergic interneurons, caused by $Na_v1.1$ epileptogenic mutations, may reduce GABAergic inhibition and cause network hyperexcitability. It was the first study to come up with a clear identification of the pathologic mechanism of a DS-associated mutation.

DS-associated $Na_v1.1$ nonsense, missense or truncating mutations are hypothesized to cause haploinsufficiency. A loss of up to 50% of functional $Na_v1.1$ protein in heterozygotes, with complete loss-of-function in channel activity and no noticeable effects on the functioning of the wild-type protein. In 2007, Kalume et al., showed that recordings from dissociated neurons lost only half of the total Na^+ current in GABAergic interneurons of heterozygous KO *Scn1a*$^{+/-}$ mice, and a smaller additional decrease was observed in homozygous KO neurons[43,44]. These results suggest a nonlinear loss of Na^+ current, that was hypothesized to depend on the compensatory up-regulation of other Na_v channels to maintain a balance (e.g., $Na_v1.3$ was found to be upregulated in

hippocampal GABAergic neurons of *Scn1a*$^{+/-}$ mice). However, a net negative effect of $Na_v1.1$ mutants was still observed on neuronal excitation levels.

Although DS is conventionally considered a loss-of-function disease, biophysical analysis of DS-Associated $Na_v1.1$ mutants has revealed a whole spectrum of presentations. Some variants result in an increase in channel function, others a decrease, and some a mixture of both loss- and gain-of-function[45–48]. Again, even within these variants, there's further heterogeneity in the mechanism of gain or loss-of-function observed. It is possible that some of these mutations alter the gating properties of the channel, others alter the trafficking or subcellular localization and yet others alter the interaction of $Na_v1.1$ with other molecules and proteins. Examples of mutations that altered the gating properties are:

- R1648H dramatically speeds channel recovery from the fast inactivated state.
- W1204R causes hyperpolarizing shifts in the voltage-dependence of activation and inactivation.
- R859C causes a depolarizing shift in the voltage-dependence of activation.
- T875M speeds entry into the slow inactivated state.

The different changes in gating properties caused by R1648H and W1204R are predicted to increase sodium channel function and subsequently, neuronal excitability. In contrast, the different changes due to R859C and T875M will reduce both channel function and neuronal excitability[49–53]. Thus, it is impossible to predict the functional effects a variant is going to have on a mutation unless it is fully characterized.

In addition to mutations in Na_v channels that affect gating, other mutations result in changes in protein folding or trafficking defects. The reduced trafficking of mutant ion channels to the plasma membrane is a well-studied pathophysiological mechanism for other channelopathies, including cystic fibrosis and congenital long QT syndrome, resulting from mutations in the cystic fibrosis transmembrane conductance regulator (CFTR) and mutations in the hERG potassium channel, respectively[54]. Due to the presence of multiple sites necessary for the protein specific interactions of $Na_v1.1$ with other proteins (Figure 1) including but not limited to phosphorylation sites for Protein

Kinases A and C, binding site for Papin, ankyrin and syntrophins, the ER retention motif, 'RXR", for the ER exporting motif[55], mutations in the intracellular linker regions have long been associated with altered folding and protein expression[20,56,57]. In 2015, Bechi et al., studied 6 previously identified mutations in $Na_v1.1$ associated with DS. The mutations studied were: Y790C[58], R859C[59], M956T, W1204R[60],V1366I[61] and M1664K[62]. These mutations all caused a reduction in the current density of the channel. On further investigation, the mechanism of action was found to be altered trafficking or protein folding properties in the mutant channel. They hypothesized that some folding defective mutations can be rescuable and that the use of pharmacological chaperones or the co-expression of interacting proteins might be enough to bring back normal channel expression levels. They suggest that the co-expression of interacting proteins like the β-subunit could be important for the modulation of the effect of these mutations leading to a reduction in phenotype severity. These molecular interactions might be important for the stabilization of correct folding conformation, allowing the mutant to pass through the quality control system of the ER. The study concluded that other than Y790C and M1664K, the four other folding or trafficking defective mutants could be rescued using a combination of temperature controlled expression, pharmacological chaperones and interacting proteins[63].

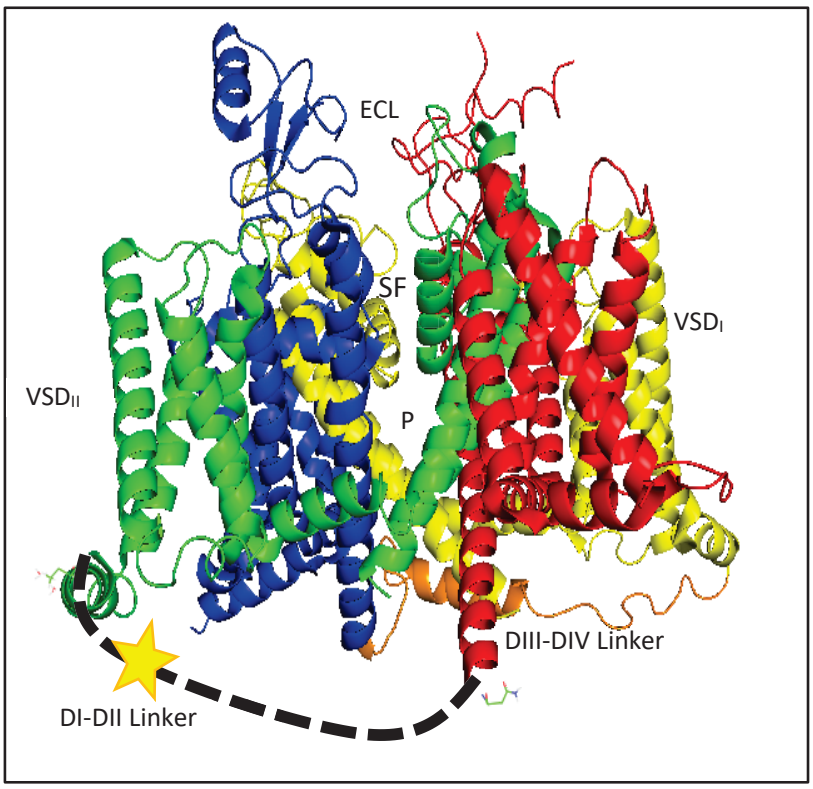

Figure 3: Location of variant in voltage-gated sodium channel ($Na_v1.1$ N722D)
The Cryo-EM structure of the mammalian voltage-gated sodium channel protein type 1, α-subunit. Each domain is made up of α-helical segments. Domains I-IV are represented by the colours red, green, blue, and yellow respectively. The star marks the site of the N722D mutation in the image where the dotted line represents the intracellular DI-DII linker region. (PDB ID: 7DTD[64]). In the figure, P=Pore forming region, SF= Ion Selectivity filter, VSD=Voltage Sensing Domain and ECL=Extracellular Loops. Structure figure prepared in PyMol[65].

1.6. Dravet Syndrome (DS)

Dravet Syndrome (DS), also known as Severe Myoclonic Epilepsy of Infancy (SMEI) is a damaging childhood epilepsy disorder associated with a high incidence of premature death and co-morbidities including delayed development, severe cognitive impairment, ataxia, circadian rhythm disorder, impaired sleep quality, and autistic-like social interaction deficits.[66,67] At around 6 to 9 months of age, the first signs of DS begin with seizures caused by an elevation in the core body temperature due to a fever, heat, or even a hot bath. This is followed by subsequent seizures within weeks that become progressively more frequent and severe throughout childhood. After six years of age, the frequency and severity of seizures are reduced but may continue into adulthood.

Seizures in DS are resistant to standard pharmaceutical therapy, even when different combinations of antiepileptic drugs are involved[68].

DS is primarily caused by either loss- or gain-of-function mutations in the *SCN1A* gene that encodes the brain voltage-gated sodium channel type-1, $Na_v1.1$.[69,70] Over 1200 mutations in *SCN1A* have been associated with DS[71]. In most cases, epilepsy is characterized by hyperactive neural signalling, which would easily be explained by the gain-of-function mutations in $Na_v1.1$, however, it may be harder to explain how a decrease in the activity of a channel that is key to propagation of neural signalling can lower seizure threshold. This contradiction has given rise to the disinhibition hypothesis as the predominant pathophysiological mechanism underlying DS. The disinhibition hypothesis states that increased neuronal excitability in disorders linked to *SCN1A* loss-of-function mutations in GABAergic interneurons may be caused by a principal impairment in the ability of interneurons to provide appropriate inhibition in neuronal networks, thus leading to an imbalance between excitation and inhibition in the brain[42,72,73]. In the last 10 years, genetic screening has become more accessible, allowing for better detection of altered genes in individuals afflicted with a disease or disorder. Prior to this, up to 30% of children with DS died before their teenage years. However, even with the availability of genetic screening, new pharmaceutical therapies, and care, up to 15% of the affected children die prematurely.

My work focuses on a patient who was diagnosed with DS and underwent genetic screening in 2019. The patient was found to have a previously uncharacterized mutation in $Na_v1.1$: the missense mutation c.2164A>G (p.Asn722Asp). I aimed to characterize the functional effects of this mutation with the hope that these insights will help inform future treatment for this child and, perhaps, others.

Chapter 2. Hypothesis And Aims:

I hypothesized that DS-associated *SCN1A* mutation, N722D in the DI-DII linker will reduce current through the channel and lead to impaired signal transmission during early development.

To test this hypothesis, I aimed to answer the following questions:

1. Does N722D disrupt voltage-dependent gating in $Na_v1.1$?
    - Using whole cell patch clamp experiments, I compared the gating properties of WT $hNa_v1.1$ and the N722D variant.
2. Does N722D disrupt channel trafficking and/or expression?
    - Using immunocytochemistry and microscopy, I characterized the expression pattern of WT $hNa_v1.1$ and the N722D variant.
3. Do changes in gating and/or channel expression predict aberrant action potential firing in developing hippocampal GABAergic interneurons?
    - Using a Hodgkin-Huxley based computational model, I compared the neuronal firing properties in both WT $Na_v1.1$and the N722D variant.

After characterizing the biophysical and expression properties of the N722D variant, I found that when compared to the WT $Na_v1.1$ channel, there is a decrease in the surface expression levels of the mutant. This reduced trafficking to the surface is enough to reduce the current density of the mutant channel and cause the loss-of-function observed. I also sought to use the results obtained from this study to discuss the clinical implications of this mutation and its consequences in afflicted individuals.

Chapter 3. Materials And Methods

The general approach for the completion of this project was to perform whole cell patch clamp recordings and immunocytochemistry experiments on Human Embryonic Kidney cells (HEK293T) transiently expressing hNa_v1.1 at room temperature (22°C). HEK293T cells are the gold standard for heterologous ion channel expression and are used here due to their low endogenous sodium channel expression properties.

3.1. Na_v1.1 subunits

Wild type (WT) human Na_v1.1 was cloned in an ampicillin/tetracycline resistant pCDM8 vector, suitable for transfection of mammalian cells. Plasmid DNA was amplified on ampicillin and tetracycline coated agar plates using competent Top10/P3 *Escherichia coli* cells from Invitrogen at 30°C. Mutant human Na_v1.1 N722D was generated using a QuikChange Lightning Site Directed Mutagenesis Kit from Agilent Technologies using the following primers:

Forward: 5’ TCTTCAAGTTCTTCTACTGTATCTGTTAGAATGCTGGCTATACTC 3’

Reverse: 5’ GAGTATAGCCAGCATTCTAACAGATACAGTAGAAGAACTTGAAGA 3’

Mutant DNA was amplified on ampicillin and tetracycline coated agar plates using the same method as for WT. The entire coding region was sequenced (Genewiz, Azenta Life Sciences) following DNA purification of both the WT and N722D mutant plasmids to ensure no unintended sequence rearrangement took place.

3.2. Cell Culture

Human Embryonic Kidney cells (HEK293T) were maintained in Dulbecco’s Modified Eagle’s medium (DMEM-Invitrogen) supplemented with 10% Foetal Bovine Serum (FBS-HyClone) in a humidified 5% CO_2 environment at 37˚C (HEPA Class II CO_2 Incubator) on 100 mm tissue culture dishes. Culture media was changed twice a week, and cells were split twice a week to avoid 100% confluency.

3.3. Transfection

For electrophysiology purposes, $Na_v1.1$ and β1 were transiently transfected into HEK293T cells prior to each recording. Stock culture cells from 100 mm dishes were plated onto 6-well plates once they reached 60-70% confluency. After the 6-well plates reached 40-50% confluency, HEK293T cells were transfected with 1 µg of $Na_v1.1$, 0.5 µg of β1 and 1 µg of eGFP DNA or 1 µg of $Na_v1.1$ N722D, 0.5 µg of β1 and 1 µg of eGFP DNA according to PolyFect transfection protocol (Qiagen, #301105). Transfected cells were plated onto coverslips in a 35 mm Petri dish. Recordings were performed the morning after plating on coverslips to ensure adequate time for production and trafficking of proteins. Green fluorescent protein was used as a marker for successfully transfected cells, and only fluorescing cells were patched on and visualized.

For immunostaining purposes, HEK293T cells were transfected with 1 µg of $Na_v1.1$ WT or $Na_v1.1$ N722D mutant DNA, along with 1 µg BFP-ER plasmid, 0.5 µg of β_1 subunit and 0.5 µg of nuclear localized eGFP plasmid DNA. Both, the BFP-ER construct and nuclear eGFP construct were generously provided by Dr. Damon Poburko (Simon Fraser University, Burnaby, BC) Transfected cells were plated on Poly L-Lysine (50 µg/mL) coated 12 mm coverslips in a 12-well plate 24 hours post-transfection and left overnight to allow adequate time for channel trafficking and expression.

3.4. Electrophysiology

Cells were visualized using a Leica DM IL LED inverted microscope (Leica Microsystems, Wetzlar, Germany). A piezoelectric micromanipulator, Burleigh PCS-250 (Exfo/Thorlabs) was used to position the patch pipette. All whole cell current recordings were made using an EPC-9 patch-clamp amplifier and digitized using an ITC- 16 interface on an iMac running Patchmaster (HEKA Elektronik, Lambrecht, Germany). Data was low pass filtered at 5kHz and sampled at 50KHz (20µs).

Pipettes were fabricated from borosilicate glass capillaries (Sutter Instruments) using a model P-1000 puller (Sutter Instruments) and fire polished on a MF-830 microforge (Narishige Japan) to a final tip resistance of 1.0-3 MΩ. Pipette (intracellular) solution was composed of the following (in mM): 120 CsF, 20 CsCl, 10 NaCl, and 10 HEPES adjusted

to pH 7.4 with CsOH. Extracellular bath solution was composed of the following (in mM): 140 NaCl, 4 KCl, 2 CaCl2, 1 MgCl2, 10 HEPES titrated to pH 7.4 with CsOH.

Transfected cells were allowed to remain in bath solution at room temperature for at least 10 min prior to gigaseal formation. Only recordings with an access resistance of less than 3.5 MΩ were included in data analysis. Series resistance compensation up to 80% was used to minimize voltage errors.

3.5. Immunocytochemistry

Transfected cells were fixed using 4% Paraformaldehyde (PFA) in phosphate-buffered saline (PBS) for 10 min at room temperature and washed 3x with PBS. This was followed by permeabilizing cells using 0.2% Triton-X100 for 10 mins, washing 3x with PBS and incubation with 2% BSA for 1 hour at room temperature. The cells were then incubated overnight with primary antibodies specific to $Na_v1.1$. Cells were washed 3x with PBS the next day followed by incubation with secondary antibodies for 1 hour at room temperature. More details about the antibodies used can be found in Table 1. After washing, cells were mounted onto glass slides using ProLong Diamond Anti-fade mountant (Thermo Fisher, #P36961). Images were collected using a Zeiss LSM-880 confocal microscope at 63x magnification. Analysis was performed using the Zen Blue image analysis software (Zeiss Zen 3.3). Mean fluorescent intensity was collected for transfected WT or N722D mutant transfected cells. Intensity values were recorded after subtraction of background intensity levels. Data was represented as an increase in intensity relative to background noise.

3.6. Western Blotting

3.6.1. Preparation of lysates

Cells were lysed in RIPA buffer (30 mM Tris-HCl, pH 7.4, 150mM NaCl, 1% octylphenoxypolyethoxyethanol (IGEPAL), 0.5% sodium deoxycholate, 0.1% sodium dodecyl sulfate (SDS), 2mM ethylenediaminetetraacetic acid (EDTA), 1mM phenylmethylsulphonyl fluoride (PMSF), 10 μg/ml leupeptin, 1 μg/ml aprotinin, 25 mM β-glycerophosphate, 10 μg/ml pepstatin, 1mM Na_2MoO_4, 1 mM Na_3VO_4). Protein concentrations were determined using the bicinchoninic acid (BCA) assay (Thermo

Fisher Scientific Pierce, #TH269546). Samples (120 μg/lane) were prepared for sodium dodecyl sulfate polyacrylamide gel electrophoresis (SDS-PAGE) by adding 1⁄4 volume of 5X reducing SDS-PAGE sample buffer (312.5mM Tris-HCl, 10% glycerol, 11.5% SDS, 500 mM dithiothreitol (DTT), pH 6.8, 0.1% bromophenol blue).

3.6.2. SDS PAGE and Immunoblotting

Samples were heated in a boiling water bath for 5 min prior to being separated using a 1.5-mm thick, 8% polyacrylamide (Bio-Rad Laboratories) mini-gel. The BenchMark Prestained Protein Ladder (7 μl per well; Invitrogen Life Technologies) was used for molecular weight standards. The gels were prepared according to standard lab procedures[74] and run in a dual vertical mini-gel apparatus (CBS Scientific, Del Mar, California) at 135 V for 2 hrs. Following this, the separated proteins were transferred onto a nitrocellulose membrane at 115 V for 2 hrs using a Bio-Rad Mini Trans-Blot apparatus. In general, the blots were blocked with 5% skim milk powder in Tris-buffered saline (TBS) for 30 min at room temperature. Primary antibodies were diluted in 5% BSA in TBS and then incubated with the blots for 16-24 hr at 4°C. Secondary antibodies were diluted in 5% BSA in TBS and added for 1 hr at room temperature. The primary and secondary antibodies are listed in Table 1. Immunoreactive bands were visualized using Radiance Enhanced Chemiluminescence Reagent (Azure Biosystems, #AC2010) and a C-digit blot scanner (Li-cor). Protein band signal intensities were quantified using Image Studio Lite (Li-cor).

Table 1: Antibodies Used

Antibody Used	Manufacturer	Catalogue Number	Working Dilution
Anti-Brain type I Voltage gated sodium channel	Alomone Laboratories	ASC001	1:275
Anti-Brain type I Voltage gated sodium channel	EMD Millipore	AB5204	1:200
Anti-Vinculin	Sigma-Aldrich	V9131	1:1000

Alexa Fluor 555 Plus goat, anti-rabbit IgG	Invitrogen	A32727	1:1000
Alexa Fluor 647 goat, anti-rabbit IgG	Invitrogen	A32733	1:500
Horseradish peroxidase conjugated goat, anti-rabbit IgG	Bio-Rad	1706515	1:3000
Horseradish peroxidase conjugated goat, anti-mouse IgG	Bio-Rad	1706516	1:3000

3.7. Statistical Analysis

All data are represented as mean ± standard error of mean (SEM). Statistical testing was performed via unpaired, two-tailed Welch's t-test for normally distributed data where n indicates the number of cells and N indicates the number of replicates. All electrophysiological data analysis was done on Fitmaster (HEKA Elektronik, Lambrecht, Germany) and Igor Pro (Wavemetrics, Oregon, USA) running on an iMac (Apple Inc., CA, USA). All data analysis for statistics was performed and graphed using GraphPad 7 (GraphPad Prism, San Diego, CA, USA). Statistical significance was evaluated at $p < 0.05$ and p-values of significance are reported in-text where appropriate.

3.8. Action Potential Modelling

Action potential firing of a neuron caused by WT $Na_v1.1$ and the N722D mutation was studied using a modified Hodgkin-Huxley computational model. The model was adapted to fit the dynamic properties of regular spiking cortical inhibitory neurons. (Pospischil, M et al., 2008). The detailed method is described in Peters et al., 2016[51]. The alteration in peak current density caused by N722D was implementing by multiplying the peak channel conductance value, g_{Na}, by 0.36, reflecting the average decrease in current density at -10 mV in $Na_v1.1$ N722D channels. Single compartment models of neurons were simulated with two different regimes. First, injections of current stimulus steadily increasing from 0.002 to 400 pA were used to study membrane

dynamics and action potential firing was measured. Next, a constant current injection of 15 pA was used to study the effect of the N722D variant on action potential firing at steady state.

Chapter 4. Results

4.1. $Na_v1.1$ N722D reduces peak current amplitude and peak-current density

To assess the functional consequences of the $Na_v1.1$ N722D mutation, the biophysical properties of $Na_v1.1$ WT and $Na_v1.1$ N722D sodium current were recorded using whole-cell voltage clamp. Comparison of $Na_v1.1$ WT and $Na_v1.1$ N722D mutant peak current recorded during step depolarization (Figure 4-A,B), reveals smaller current magnitudes for N722D mutant channels. The average amplitude of the maximum peak current was 874.1 pA (n = 8) for $Na_v1.1$ WT and 307.4 pA (n = 7) for $Na_v1.1$ N722D mutant channels. When compared to the WT, N722D shows a significant reduction in the peak-current amplitude values recorded at -10 mV. (p=0.02965) (Figure 4-C, Table 2). There is also a significant (p = 0.0273) reduction in the current density values of the $Na_v1.1$ N722D cells measured at -10 mV when compared to $Na_v1.1$ WT (Figure 5, Table 3)

Table 2: Mean current amplitude values

	Mean Current Amplitude (pA)	SEM	N
$Na_v1.1$ WT	874.1	207.04	8
$Na_v1.1$ N722D	307.38	52.79	7

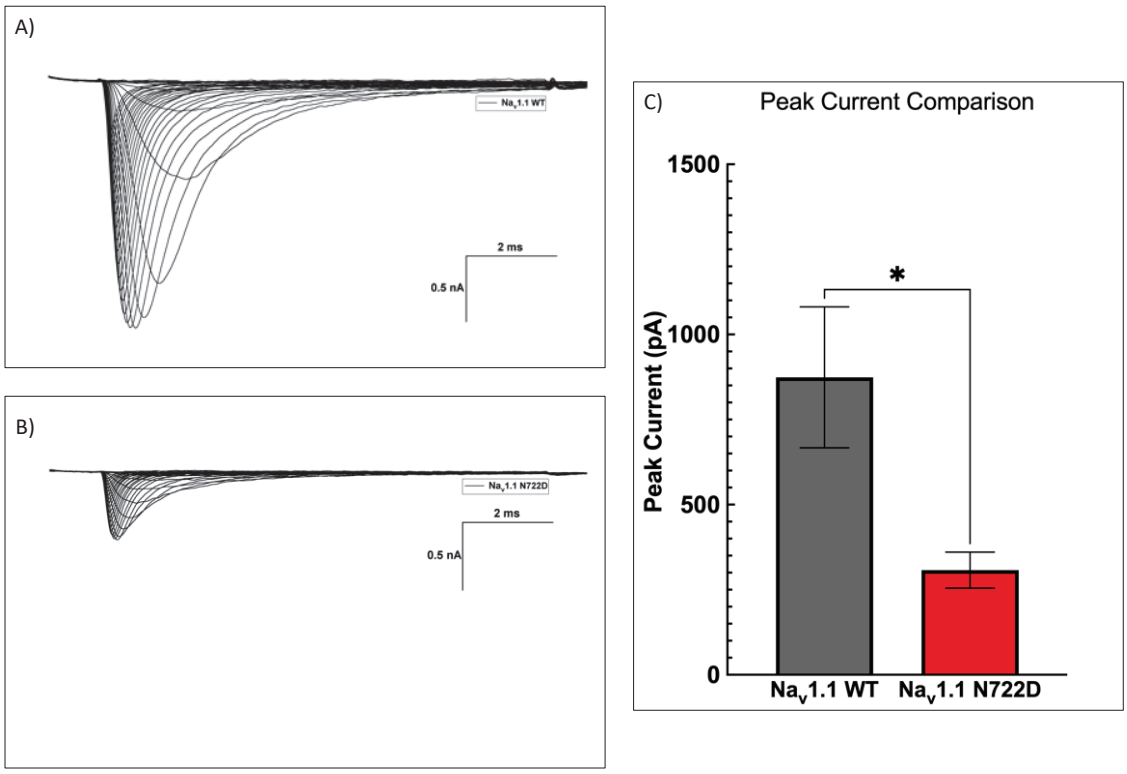

Figure 4: Na$_v$1.1 WT and N722D current traces
Representative inward macroscopic currents of Na$_v$1.1 WT (A) and Na$_v$1.1 N722D (B) cells elicited at potentials between −100 mV and +60 mV at 22 °C. Bar graph showing peak current amplitude of WT (gray) and Na$_v$1.1 N722D (red)(C). All error bars represent standard error of the mean.

4.2. $Na_v1.1$ N722D reduces peak current density through the channel

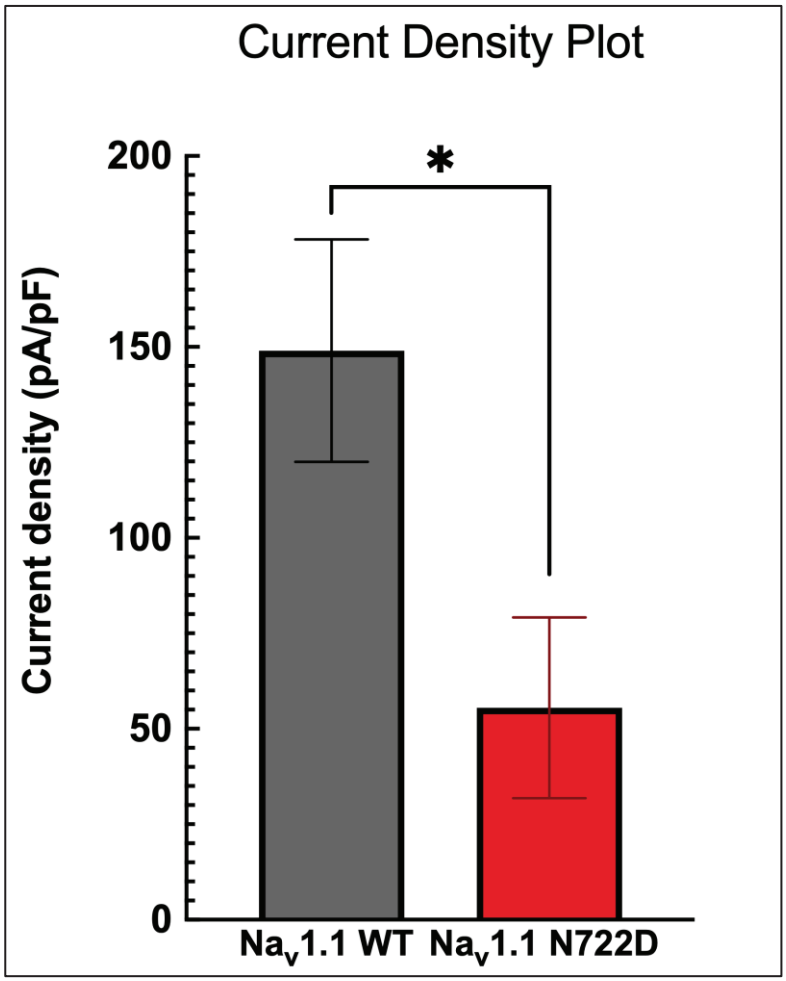

Figure 5: $Na_v1.1$ N722D shows a reduction in peak current density
Bar graph depicting current density values at -10 mV for $Na_v1.1$ WT (gray, n=8) and $Na_v1.1$ N722D (red, n=7). Data is represented as mean ± Standard error of the mean.

Table 3: Mean current density values

	Mean Current Density (pA/pF)	SEM	N
$Na_v1.1$ WT	148.67	29.23	8
$Na_v1.1$ N722D	55.50	23.67	7

4.3. Voltage Dependence of Activation is not significantly different in $Na_v1.1$ N722D

Cells were held at -130 mV and depolarized from -100 mV to +60 mV in 5 mV steps for a duration of 20 ms. Leak currents were compensated during recording with a P/4 leak subtraction protocol. This protocol measures the ohmic leak and capacity current, which is then subtracted from the voltage dependent sodium current. A series of 4 hyperpolarizing voltage steps 1⁄4 of the magnitude of those used to generate sodium current are performed after each pulse.

Channel conductance (G) was calculated from peak I_{Na} using Eqn. 1, where G_{Na} is conductance, I_{Na} is peak sodium current in response to V, the test pulse membrane potential, and E_{Na} is the equilibrium potential calculated from the Nernst equation. Conductance vs. voltage curves were fit with a Boltzmann function (Eqn. 2), where I/I_{max} is normalized current amplitude, V_m is the test pulse membrane potential, z is the apparent valence, e_0 is the elementary charge, $V_{1/2}$ is the midpoint voltage, k is the Boltzmann constant and T is the temperature in K.

Eqn 1: $G_{Na} = \frac{I_{Na}}{V - E_{Na}}$ **Eqn 2**: $\frac{I}{I_{max}} = \frac{1}{1+\exp\left(-\frac{ze_0\left(V_m - V_{\frac{1}{2}}\right)}{kT}\right)}$

No significant (p = 0.2734) shifts were observed in the midpoint values of the conductance-voltage relationship between the $Na_v1.1$ WT and the $Na_v1.1$ N722D.

Table 4: Gating parameters for conductance-voltage relationship

	$V_{1/2}$ (mV)	SEM	N
$Na_v1.1$ WT	-27.97	2.42	8
$Na_v1.1$ N722D	-31.53	1.92	7

A)

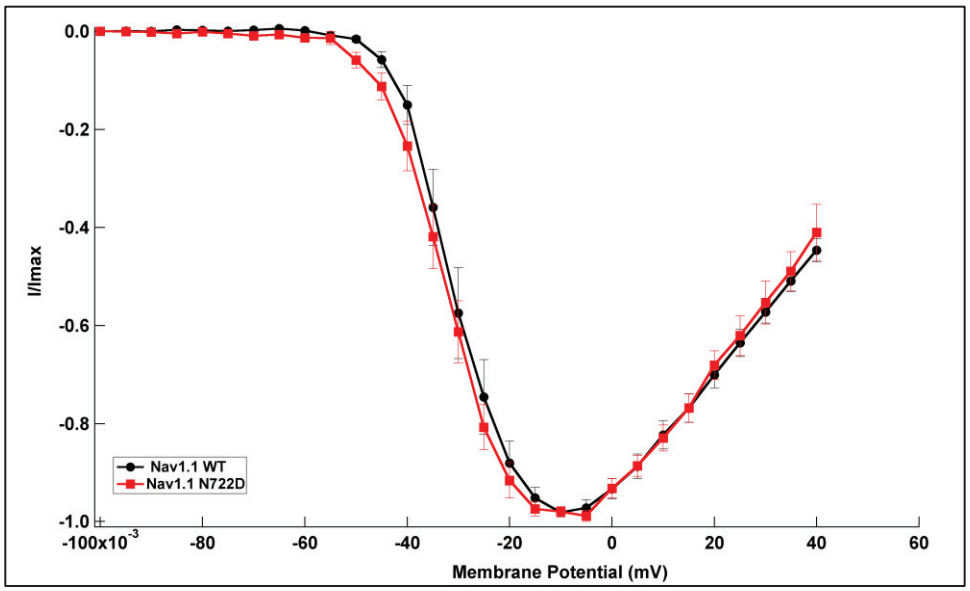

B)

:

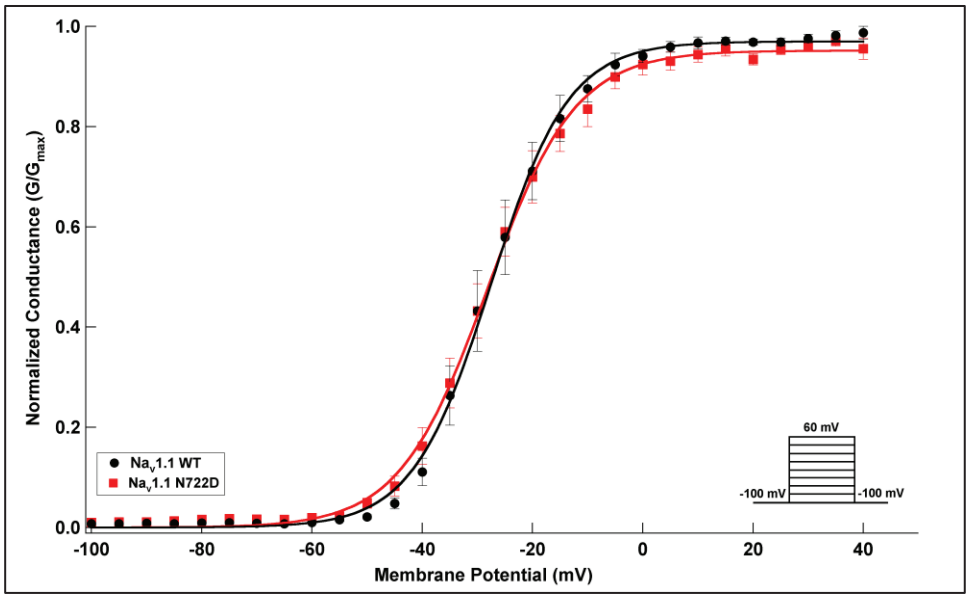

Figure 6: Voltage dependence of activation

(A) Normalized graph showing current-voltage relationships between $Na_v1.1$ WT (black) and $Na_v1.1$ N722D (red). (B) Normalized conductance curves for $Na_v1.1$ WT (black) and $Na_v1.1$ N722D (red) channels are shown at 22°C. **Inset**: Voltage protocol used to measure channel conductance.

4.4. $Na_v1.1$ N722D does not significantly alter Voltage Dependence of Inactivation

Steady-state fast inactivation was recorded as the proportion of current remaining in a test pulse following prepulses at voltages between -130 mV and +10 mV spaced at 200 ms each. Normalized current vs voltage curves were fit using a Boltzmann function (Eqn. 2). The normalized current was plotted against prepulse potential as shown in Figure 7.

No significant shifts were observed in the midpoint values of the fast inactivation voltage dependence between $Na_v1.1$ WT and $Na_v1.1$ N722D ($p = 0.4525$).

Table 5: Gating parameters for voltage dependence of inactivation

	$V_{1/2}$ (mV)	SEM	N
$Na_v1.1$ WT	-68.54	2.26	8
$Na_v1.1$ N722D	-70.90	2.30	7

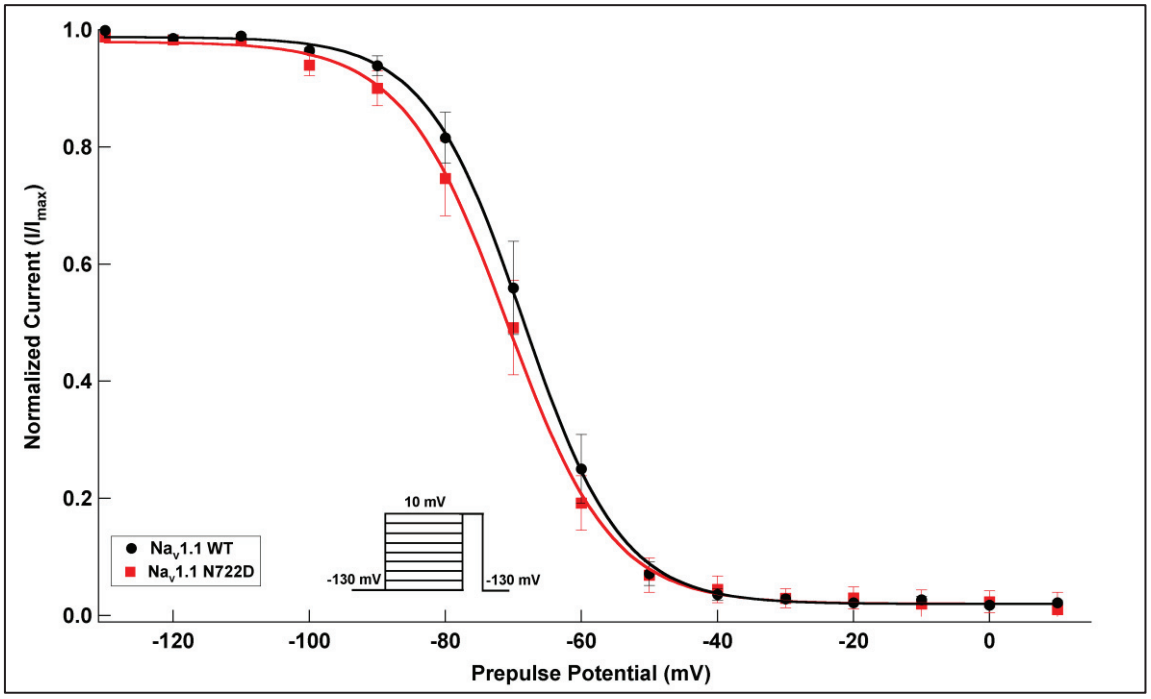

Figure 7: Steady-State Fast-Inactivation
Voltage dependence of fast inactivation for $Na_v1.1$ WT (black) and $Na_v1.1$ N722D (red) recorded at 22°C. **Inset:** Voltage protocol for measuring the voltage-dependence of inactivation.

4.5. Recovery from Fast Inactivation is not significantly different in $Na_v1.1$ N722D

The time course of recovery from fast inactivation at -90 mV was measured as the proportion of current remaining after a 200 ms depolarization to 0 mV and a recovery pulse of varying lengths to -90 mV. Normalized current was plotted against recovery time and fit using a double exponential equation (Eqn. 3), where I is current amplitude, I_{SS} is steady state current, α_1 and α_2 are the amplitudes at time 0 for time constants $\tau 1$ and $\tau 2$ and t is time.

$$\textbf{Eqn 3: } I = I_{SS} + \alpha_1 e^{-\frac{t}{\tau_1}} + \alpha_2 e^{-\frac{t}{\tau_2}}$$

$Na_v1.1$ N722D does not significantly alter the rate of recovery from fast inactivation at -90 mV (p=0.9704)

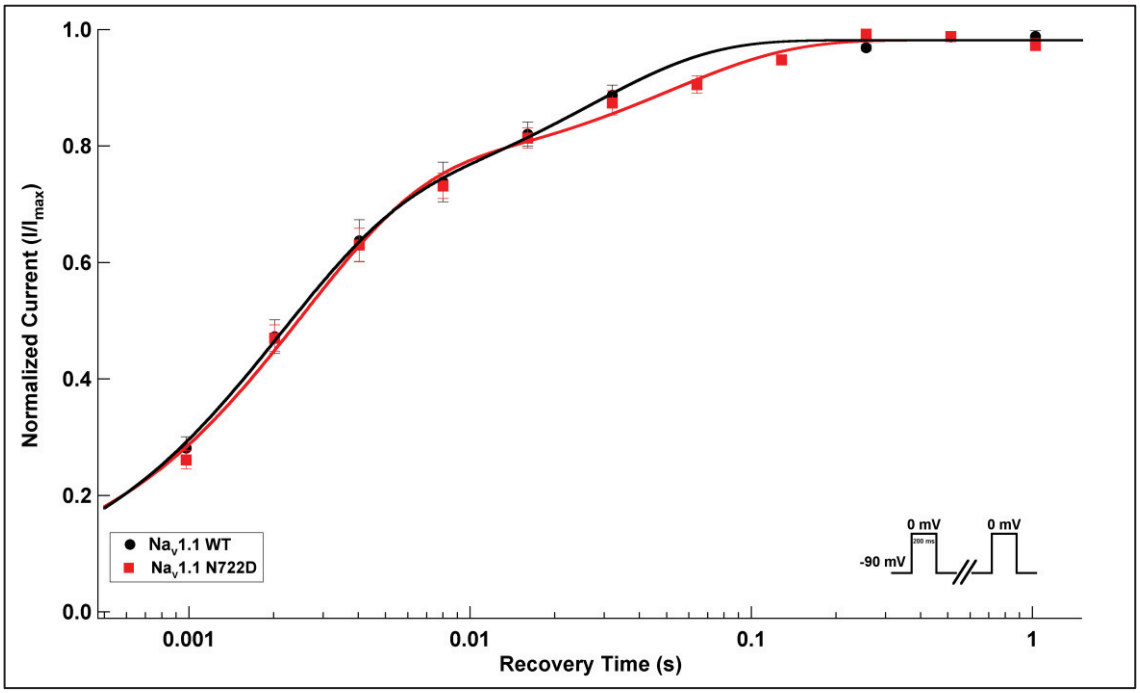

Figure 8: Recovery from Fast Inactivation
Time-course of channel recovery from fast-inactivation at -90 mV as observed in $Na_v1.1$ WT (black) and $Na_v1.1$ N722D (red) cells recorded at 22°C. Inset: Double-pulse protocol for measuring the fast inactivation recovery. All error bars represent standard error of the mean.

Table 6: Gating parameters for channel recovery from Fast Inactivation

	τ1 (s)	SEM	A1	SEM	N
$Na_v1.1$ WT	0.0057	0.00012	-22.90	0.015	8
$Na_v1.1$ N722D	0.0057	0.00093	-22.88	0.014	7

4.6. Persistent current is not significantly different in $Na_v1.1$ N722D

Persistent current (I_{NaP}) was measured as a fraction of non-inactivating current during a 50 ms pulse from -130 mV to 0 mV. The current amplitude measured at the end of the 50 ms depolarizing pulse was divided by the peak current to calculate the percentage of persistent current produced by the channel. At 22°C, there was no significant difference ($p = 0.3645$) in the fraction of non-inactivating current measured in $Na_v1.1$ N722D when compared to $Na_v1.1$ WT as seen in Figure 9 (B).

Table 7: Mean values for persistent current

	Persistent Current (% of peak)	SEM	N
$Na_v1.1$ WT	2.05	0.36	8
$Na_v1.1$ N722D	2.58	0.44	7

A)

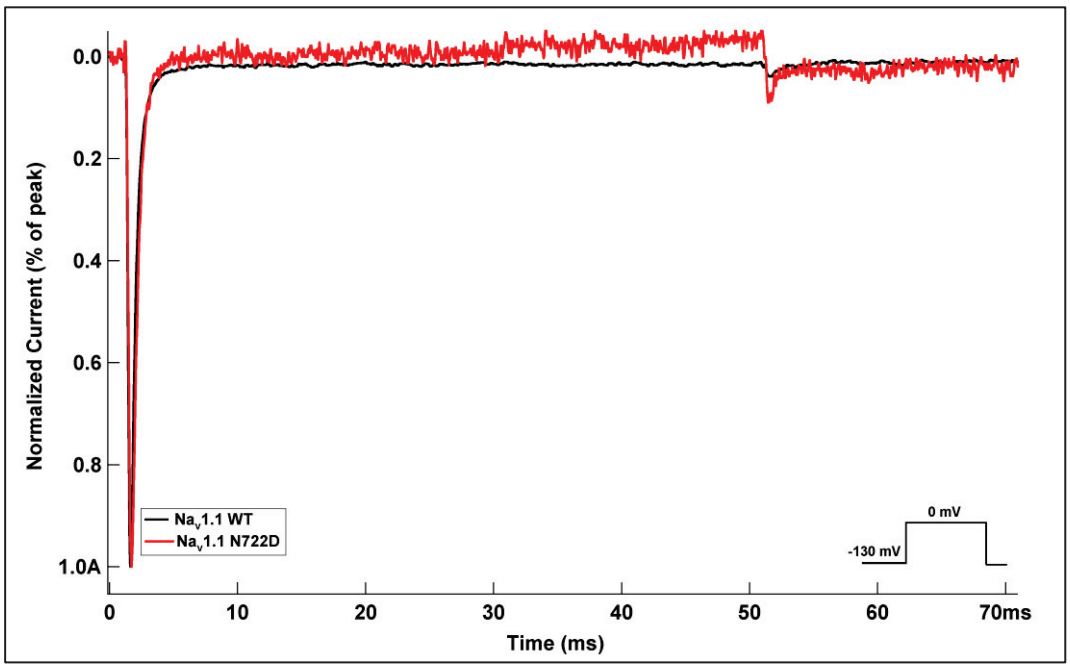

B)

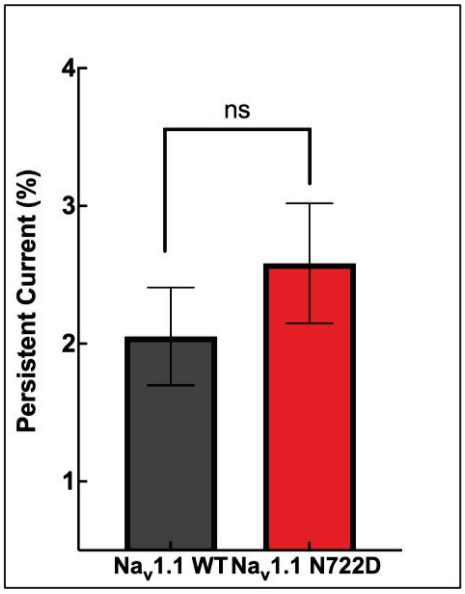

Figure 9: Persistent current

(A) Normalized sample currents at −20 mV from Na$_v$1.1 WT (black) and Na$_v$1.1 N722D (red). (B) Average fraction of non-inactivating current at −20 mV normalized to peak current for Na$_v$1.1 WT (black) and Na$_v$1.1 N722D (red). Data is represented as mean ± standard error of the mean.

4.7. $Na_v1.1$ N722D shows altered channel expression properties when compared to $Na_v1.1$ WT

To ascertain if the reduction in peak current amplitude in $Na_v1.1$ N722D cells is a reflection of a reduction in the number of channels in the plasma membrane or if it is due to the presence of a population of channels that are entirely non-functional, immunostaining analysis was performed in HEK293T cells expressing $Na_v1.1$ WT, $Na_v1.1$ N722D channels as well as other constructs including the BFP-ER tag, nuclear GFP marker and the β_1 subunit. Transfected cells were stained with antibodies against the neuronal sodium channel protein $Na_v1.1$. Cells transfected with WT *SCN1A* had a very well distinguished rim of $Na_v1.1$ surrounding the intracellular BFP-ER stain, an indicator of successful trafficking of sodium channels to the surface of the cell (Figure 10-A). Alternatively, cells transfected with N722D mutant are visibly diffused throughout the intracellular region of the cell and have minimal membrane staining for $Na_v1.1$ (Figure 10-B). This can also be seen on the channel expression profile plots (Figure 11, A and B) where the $Na_v1.1$ WT channel shows peaks at the very ends of the plot i.e. on the plasma membrane of the cell, whereas the $Na_v1.1$ N722D channel shows irregular spikes in channel intensity throughout the intracellular space further supporting my trafficking defect hypothesis.

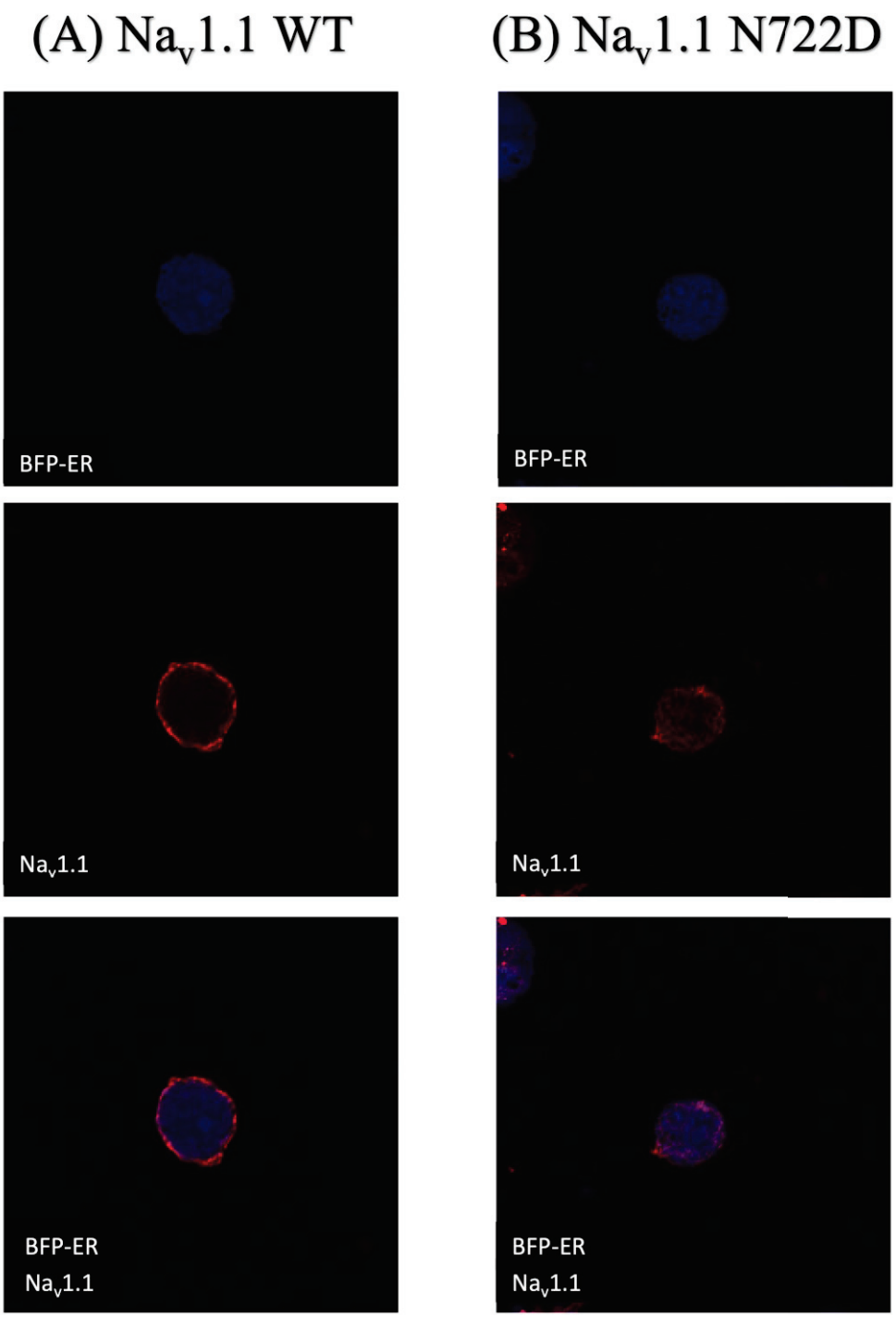

Figure 10: Visualization of Na$_v$1.1 WT and N722D expression in HEK293T cells
Representative cells depicting expression patterns of Na$_v$1.1 WT (A) and Na$_v$1.1 N722D (B) with co-expression of BFP-ER in transfected HEK293T cells.

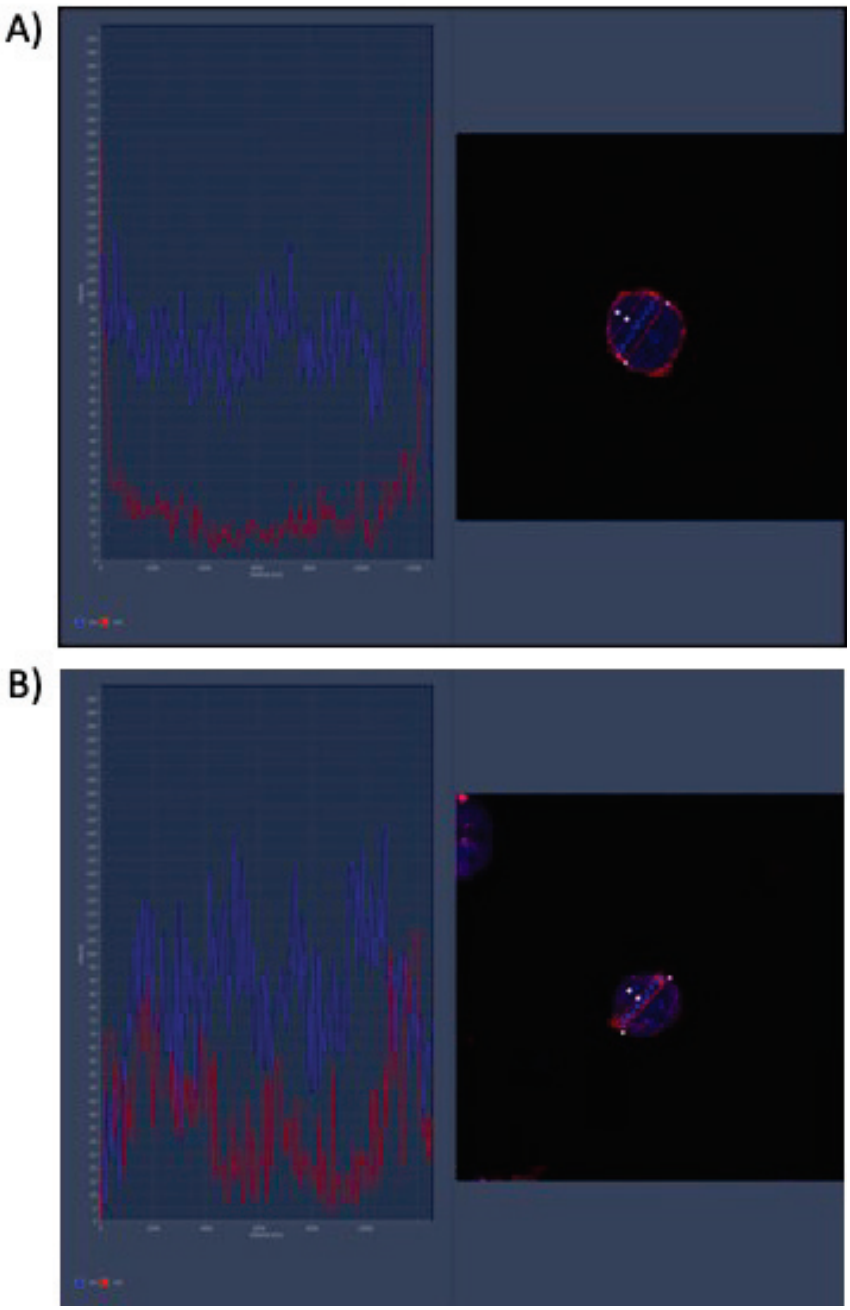

Figure 11: $Na_v1.1$ WT and N722D Channel Expression Profile Plots
(A) $Na_v1.1$ WT channel intensity values peak around the edges of the cell (red), suggesting that while the BFP-ER tag is expressed more or less-uniformly throughout the cell (blue), $Na_v1.1$ WT can only be found at the edges or on the surface of the cell. (B) $Na_v1.1$ N722D is found to be scattered throughout the intracellular space, and not specifically on the edges of the cell

4.8. $Na_v1.1$ WT transfected cells show higher fluorescence intensity on cell surface when compared to $Na_v1.1$ N722D transfected cells.

To further quantitatively verify whether expression was altered in the $Na_v1.1$ N722D mutant channels, I measured cell surface immunofluorescence in HEK293T cells. Cells were transfected with both, $Na_v1.1$ WT and $Na_v1.1$ N722D channels. The mean fluorescent intensity values for both channels were recorded from the surface of 60-65 cells in three independent experiments and plotted after subtraction of background fluorescence intensity. $Na_v1.1$ WT cells show a significantly higher mean fluorescent intensity than cells transfected with $Na_v1.1$ N722D (Figure 12; Table 08) ($p < 0.0001$)

Table 8: Mean fluorescence intensity values for $Na_v1.1$ WT and N722D

	Mean Fluorescence Intensity (pixels)	SEM	n, N
$Na_v1.1$ WT	46.99	1.489	65, 3
$Na_v1.1$ N722D	36.89	1.936	60, 3

n refers to number of cells analyzed, N refers to the number of separate experiments run.

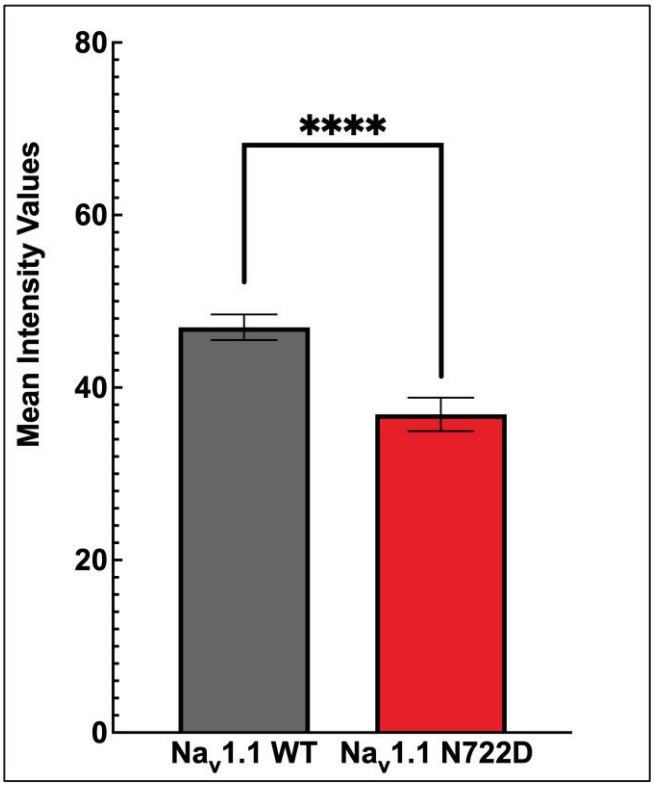

Figure 12: Comparison of cell-surface fluorescent intensities of Nav1.1 WT and N722D

Bar graph depicting the mean fluorescent intensities of $Na_v1.1$ WT (n=65, N=3) and $Na_v1.1$ N722D (n=60, N=3) mutant channels as observed from immunostaining experiments. Data is represented as mean ± standard error of the mean. ****Statistically significant difference ($p < 0.0001$) in Welch's t-test comparing WT to N722D.

4.9. Whole-cell lysate western blots do not show altered $Na_v1.1$ WT and $Na_v1.1$ N722D protein levels

I used a whole-cell lysate western blot to ensure that the differences in intensity values reported in the immunostaining experiment were due to altered expression properties and not due to differences in transfection quantities. Before lysing, the cells were transfected using the same quantities of DNA and allowed to express proteins for the same amount of time as was done before whole-cell patch clamping and immunostaining protocols. After lysing and protein estimation, 120 ng of each, $Na_v1.1$ WT and $Na_v1.1$ N722D was loaded into an 8% SDS-PAGE gel and allowed to be separated. After separation, the bands were transferred onto a PVDF membrane before blocking and probing with primary $Na_v1.1$, Vinculin, and secondary Abs (Table 01). The membrane was then visualized (Figure 10-A) and protein band intensities were measured (Figure 13-B). There was no significant difference ($p = 0.8057$) noted among the signal intensities of the $Na_v1.1$ WT and $Na_v1.1$ N722D bands or the band intensities of the loading control, Vinculin ($p = 0.7528$).

Table 9: Mean band intensity values from immunoblots

	Mean Signal Intensity (pixels)	SEM	N
$Na_v1.1$ WT	264000	17009.8	3
$Na_v1.1$ N722D	271333.33	21364.56	3
$Na_v1.1$ WT- Vinculin	2266666.67	97353.88	3
$Na_v1.1$ N722D- Vinculin	2216666.67	107285.85	3

A)

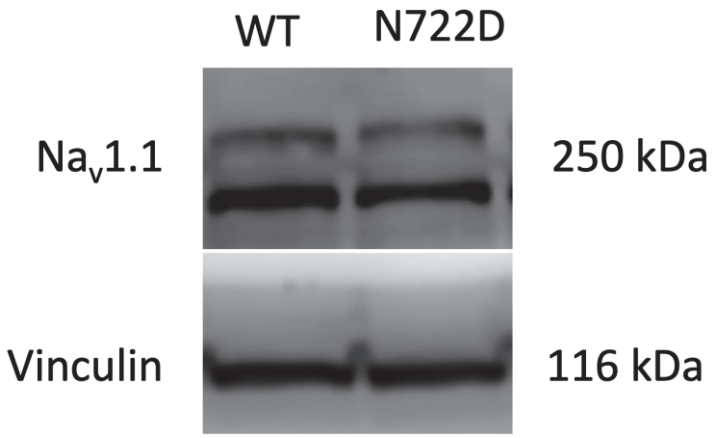

B)

Na$_v$1.1 Band intensity

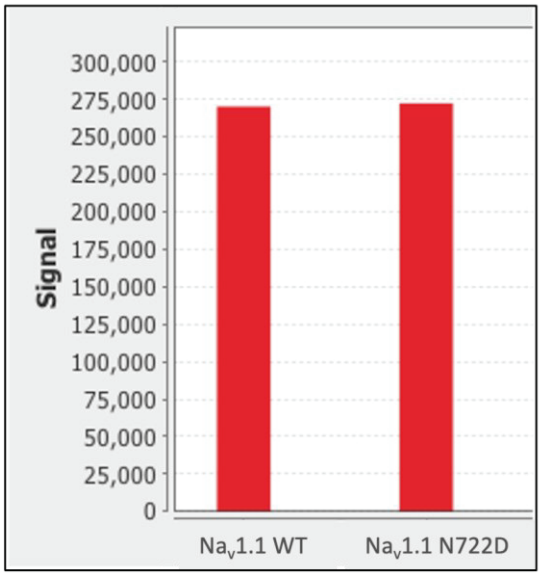

Vinculin Band intensity

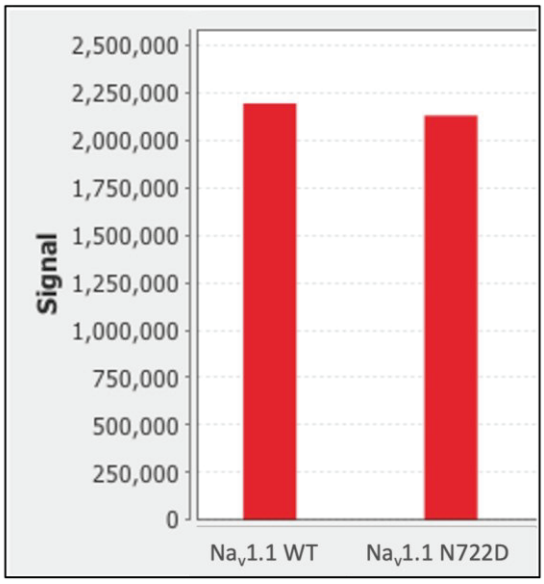

Figure 13: Representative immunoblots
Western blot probed with Anti-Na$_v$ 1.1 Ab depicting equal levels of protein expression (A) when compared to loading control Vinculin (N=3). Representative graphs showing measured band intensities (B). No significant differences were observed in band intensities between the Na$_v$1.1 WT and Na$_v$1.1 N722D mutant.

4.10. Action Potential modelling of $Na_v1.1$ N722D neurons shows altered firing properties.

To demonstrate the effect of the $Na_v1.1$ N722D mutation on firing of inhibitory GABAergic neurons, I used the Hodgkin-Huxley based cortical neuron model to visualize any aberrations in firing properties when compared to $Na_v1.1$ WT neurons. The model was modified based on electrophysiological data obtained, particularly the differences in peak-current density values. The results obtained were then plotted to visualize differences as seen in Figure 14-A and B. $Na_v1.1$ N722D neurons show a difference in three key areas, i) they show a delay in the initiation (delayed onset) of action potential firing, and ii) they have a smaller range of voltage while firing and iii) when stimulated using the same amplitude of current, they fire at slower frequencies when compared to the WT (Figure 15-A). This observation further supports the hypothesis of $Na_v1.1$ N722D being a loss-of-function mutation.

A)

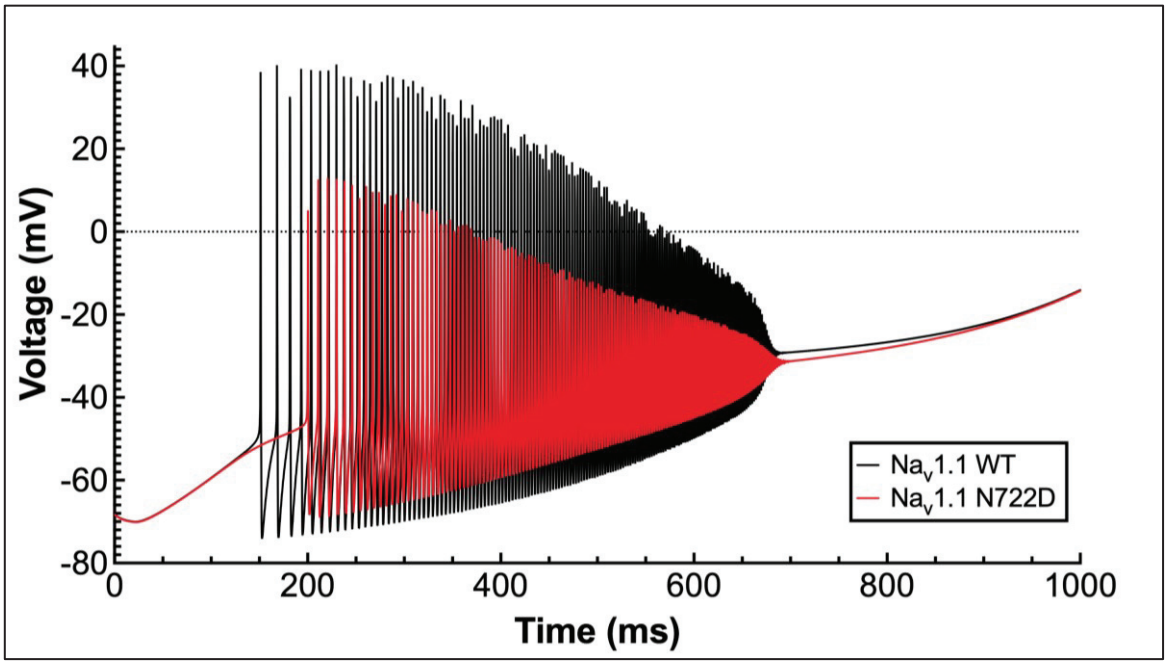

B)

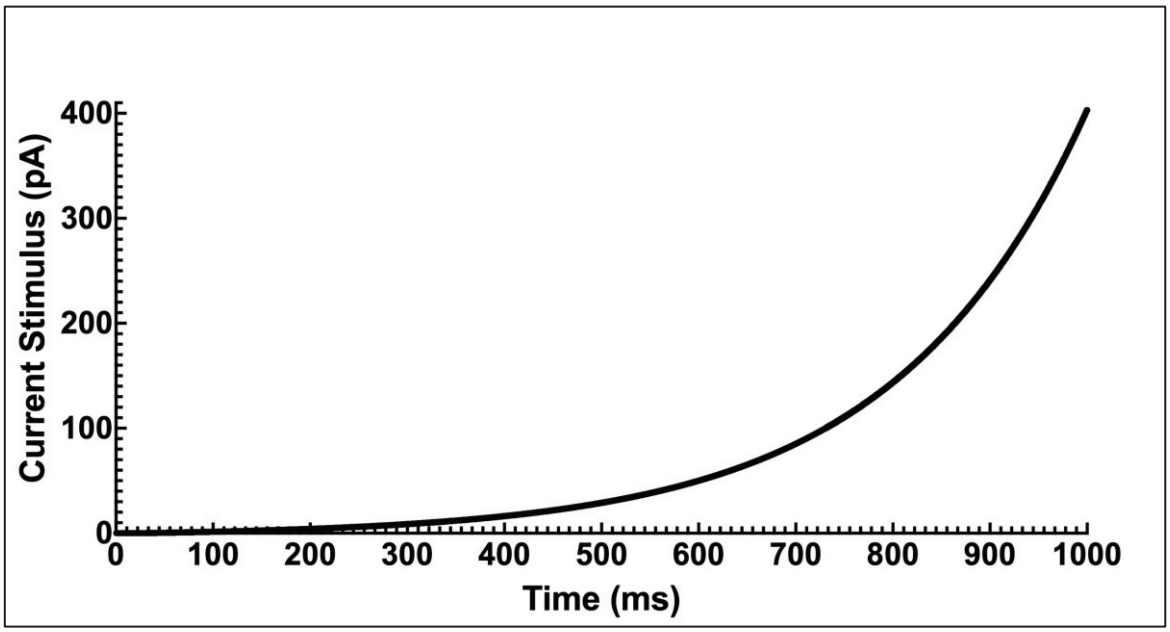

Figure 14: Action Potential Modelling of Na$_v$1.1
GABAergic Inhibitory neuron action potential model of Na$_v$1.1 WT (black) and Na$_v$1.1 N722D (red) depicting response of neurons (A) to a constantly increasing stimulus of injected current from 0.002 pA to 400 pA (B)

A)

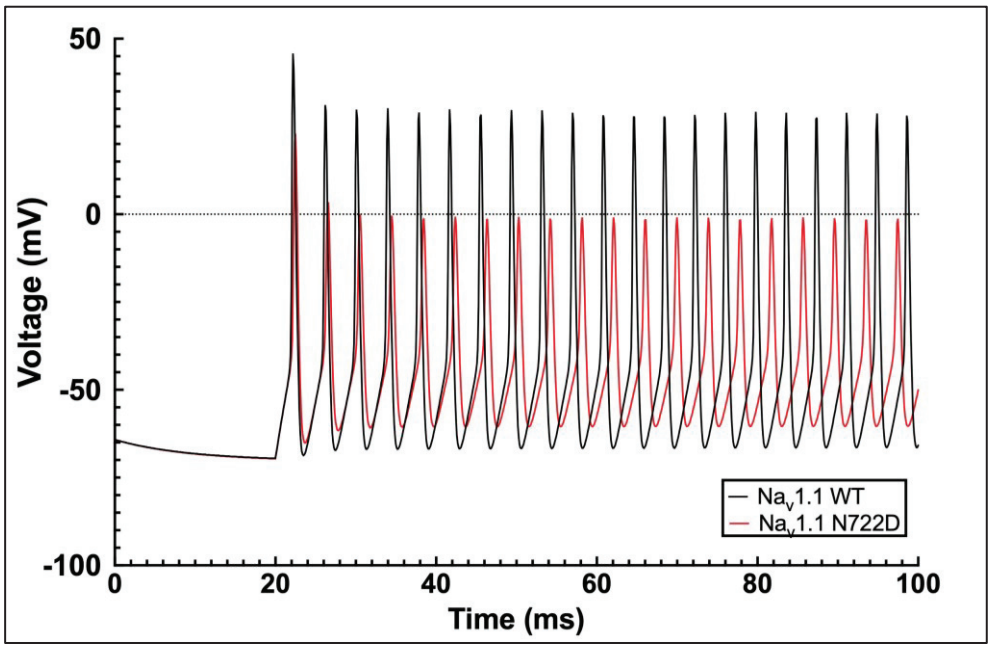

B)

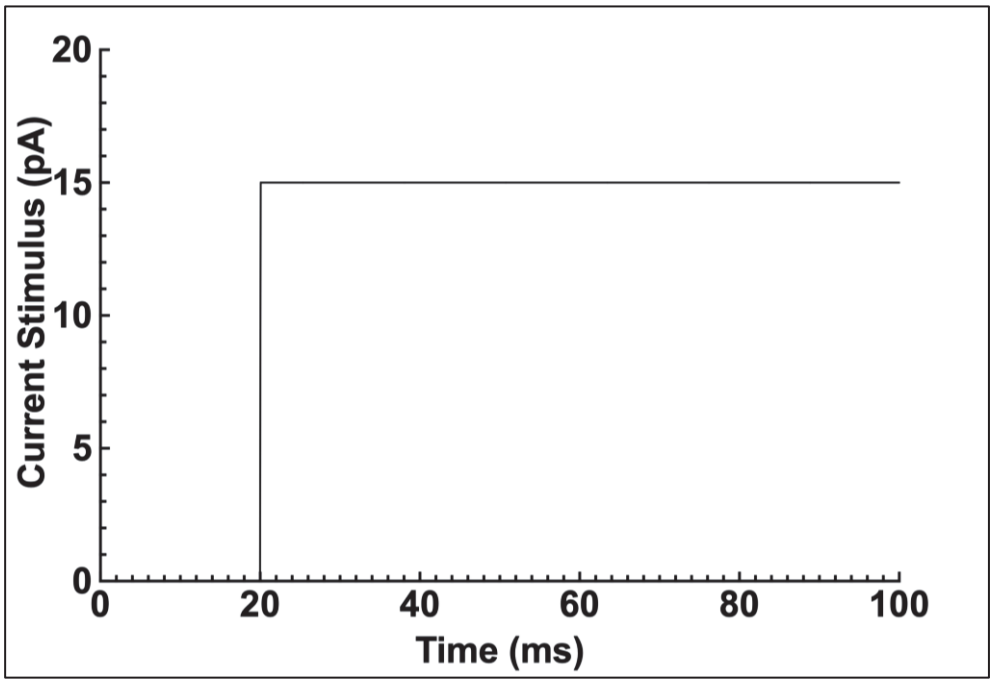

Figure 15: Action Potential Modelling of Na$_v$1.1 Using Set Stimulus :
(A) GABAergic Inhibitory neuron action potential model of Na$_v$1.1 WT (black) and Na$_v$1.1 N722D (red) depicting response of neurons to a set stimulus of 15 pA. (B) A depiction of the set stimulus of 15 pA.

Chapter 5. Discussion

5.1. $Na_v1.1$ and Dravet Syndrome

Mutations in the *SCN1A* gene that codes for voltage gated sodium channel, $Na_v1.1$ account for ~80% of all DS cases[71,75–77]. The class of DS-associated mutations ranges from nonsense and missense to frameshift and splice site mutations. The difference in type of mutations also implies that the functional property they alter varies on a case by case basis[32]. DS is most often associated with the loss-of-function in $Na_v1.1$ activity[78]. However, that is not always the case. Some DS-associated mutations were characterized as a gain-of-function or a mixed gain- and loss-of-function[51,79,80]. Due to this heterogeneity, each DS-associated mutation must be individually characterized to understand the relationship between the phenotype observed and its genotype and to develop individualized strategies for treatment. It is likely that many of these mutations alter - but not entirely abolish - channel function, possibly by affecting the conducting properties of the channel, trafficking, subcellular localization, or through interactions with other molecules.

In this study, I discuss an infant boy with a clinical diagnosis of DS who presented with seizures first at 14 months of age and has had them unprovoked ever since. Genetic screening revealed a mutation (pN722D) in the *SCN1A* gene. To understand the functional effects of the N722D mutation, I characterized the mutation using a combination of patch-clamping, immunocytochemistry with a focus on expression studies, and computational modelling. Due to the presence of multiple phosphorylation sites in the DI-DII linker region near the site of the mutation[20,81,82], I hypothesized there would be an effect on channel localization and trafficking properties in $Na_v1.1$ N722D. My electrophysiology results show that the only biophysical property in N722D that differs from WT $Na_v1.1$ is a significant reduction (almost 3-fold) in the peak current density of the mutant channel at -10 mV. No other activation or inactivation parameters were affected. These results suggest that the mutation is a loss-of-function mutation that may be altering the trafficking properties of the channel.

5.2. $Na_v1.1$ N722D alters trafficking properties of the channel

As seen in the results, there is a reduction in the number of mutant channels available on the surface of the plasma membrane in transfected HEK293T cells. However, when channel expression profiles were plotted, we observed a stark difference in where the two Na_vs were found. This was compared with expression properties of the BFP-ER tag that was co-transfected into the HEK293T cells. WT $Na_v1.1$ had peak expression values on the edges of the plot, a reflection of its expression within the plasma membrane of the cell. In contrast, the N722D mutant channels are scattered in throughout the intracellular space. When surface channel intensity levels were plotted and compared, $Na_v1.1$ N722D levels were found to be significantly lower than those of WT $Na_v1.1$.

To further confirm that the differences in intensity values were due to actual differences in expression rather than differences in transfection, whole cell lysate western blot analysis was carried out in three independently transfected experiments. Results from whole cell lysate immunoblotting band signal intensity values suggested no significant differences when normalized to the loading control (Vinculin).

Put together, these data suggest a trafficking defect in $Na_v1.1$ N722D which explains the loss-of-function shown in the significant decrease in peak current density. Extending these results to the inhibitory GABAergic interneurons in which $Na_v1.1$ are found, impaired trafficking leading to a decrease in current density would result in a subsequent decrease in the release of GABA (inhibitory) neurotransmitter and a subsequent increase in overall brain excitability. It is therefore reasonable to surmise that loss-of-function underlies DS in this and other similarly affected individuals.

The trafficking defect in N722D could be caused by alterations in the post-translational modifications of $Na_v1.1$ and subsequent reduction in surface expression levels due to quality control checkpoints in the ER. Every step in the early stage Na_v biosynthesis process (exiting the ER and Golgi apparatus to reach to the plasma membrane) is crucial for the development of healthy neuronal networks in humans[54,56]. It is therefore not surprising that several disease-related mutations in $Na_v1.1$ are caused by defects in the trafficking pathway[54,56]. Missense or truncation mutations in integral

membrane proteins like voltage-gated sodium channels can disrupt intrinsic protein folding and assembly that in turn leads to abnormal protein trafficking or degradation during biosynthesis[83]. I hypothesize that this observation stands true for the N722D mutation located in the DI-DII linker region in $Na_v1.1$. The intracellular linker contains sites for interactions of Na_vs with important modulatory and regulatory proteins (Figure 1). These include phosphorylation sites for Protein Kinases A and C, binding site for Papin, ankyrin and syntrophins, the ER retention motif, 'RXR', and for the ER exporting motif[55]. Studies in $Na_v1.5$ report that for the successful export of a fully properly folded channel protein from the ER, it needs to pass the quality control mechanism involving binding of 14-3-3 proteins to the RXR motif[84]. This binding facilitates the anterograde transport of the folded protein from the ER to the Golgi apparatus for further post-translational modifications[85]. However, if this site is mutated, preventing the binding of 14-3-3, the channel protein is marked for degradation by the ER control mechanism and destroyed before making it to the plasma membrane. While the mechanism of action of the RXR site in $Na_v1.1$ has not been fully studied yet, considering the sequence and homology similarities to $Na_v1.5$, it could operate in a similar manner. Furthermore, there is an overlap in the RXR motif site and the site for PKA phosphorylation in Na_vs. In 2003, Carr et al., reported that the activation of PKA reduced peak currents of $Na_v1.1$ without significantly altering any of the steady state voltage dependent properties of the channel[86]. The phosphorylation of these sites overrides ER retention and marks the channel protein for degradation or intracellular retention possibly by the interaction with A-kinase anchoring proteins (AKAP)[87]. This claim however needs to be investigated further before any conclusions can be drawn.

Studies show that the pharmacological rescue of these trafficking impaired mutant channels is possible and has been demonstrated in other channelopathies[88,89].These studies suggested the incubation of standard anti-epileptic drugs with transfected cells for at least 16 hours to rescue cell surface channel expression and functionality. While there was rescue of cell surface expression, however, there were also adverse effects observed including an increase in persistent sodium current due to the mutant[54]. Due to lack of information about the molecular machinery involved in various stages of the post-translational modification pathways in $Na_v1.1$, the exact reason for the instability of misfolded proteins not being properly trafficked to the surface of the cell is not yet known. There is some reasoning to support

the hypothesis that misfolded proteins have altered dynamics and kinetics, which results in the modification of stable conformations in the protein domains containing the mutation[90]. A better understanding of the complexity of Na_v localization, functional reliance on this localization, and their interactions with modulatory proteins will shed light on the role they play in neuronal activity of health and disease.

5.3. Reduced excitability in GABAergic interneurons and clinical implications

Computational modelling of $Na_v1.1$ N722D neurons based on electrophysiological properties of the channel suggests a decrease in action potential firing number, frequency, and amplitude when compared to the same model of $Na_v1.1$ WT neurons. The decrease in action potential firing properties in $Na_v1.1$ N722D mutant inhibitory neurons indicates that there is a substantial impairment in the excitability of these neurons. This result is suggestive of the need for larger graded potentials to reach the same action potential firing threshold observed in WT neurons. I postulate that this significant alteration of firing properties and excitability in $Na_v1.1$ N722D mutant interneurons is an important causative factor underlying the epileptic phenotype observed in this patient.

GABAergic neurons in the hippocampus and the cortex play a vital role in the gate-keeping function of excitatory pyramidal cells[91]. Interneurons have been known to regulate and control the inputs to pyramidal cells, the timing and rate of firing in pyramidal cells, the synchronization of neural network oscillations, and the regulation of inputs to the circuit of neighbouring interneurons[92–98]. These important roles are accomplished by responding to dynamic changes in excitation levels while maintaining a balance in the excitatory and inhibitory signals to sustain information transfer and prevent runaway excitation at the same time. The spatial and temporal precision required for these functions suggests the need for fully functional neuronal firing in the cortex and hippocampus.

Furthermore, alterations or malfunctions in the firing properties of inhibitory GABAergic interneurons has long been associated with neurodevelopmental and

neurocognitive disorders ranging from epilepsy and schizophrenia to anxiety and autism spectrum disorders[99–103]. Additionally, other types of inhibitory neurons play different roles in the maintenance of network activity in different parts of the brain. Parvalbumin (PV) positive basket cells are ideally positioned to provide strong and fast feed-forward inhibition to adjacently located pyramidal cells in the cortex[104,105]. These interneurons can trigger and maintain the high-frequency gamma oscillations within networks of pyramidal neurons in the cortex[106–109]. Gamma oscillations play a vital role in the maintenance of attention, working memory and refinement of executive functions[110,111]. Thus, any dysfunction in PV-positive GABAergic interneurons caused by $Na_v1.1$ N722D underlies loss of gamma oscillations, thereby resulting in abnormalities in working memory and executive function[112–115].

Somatostatin (SST) positive Martinotti cells in the cortex play a vital role in dampening the excitation of pyramidal cells during high activation states. Studies hypothesize that these interneurons could also play a role in pacing cortical pyramidal cells in the theta range[102,116–118]. Alteration of striatocortical GABAergic circuits has also been associated with the abnormal autistic-like behavioural phenotype observed in mice that show increased anxiety and altered socialization[103,119–121]. Deletion of $Na_v1.1$ to cause haploinsufficiency in GABAergic Purkinje neurons and the subsequent alteration in action potential firing of these neurons[122] has been shown to be sufficient to cause ataxia, one of the first co-morbidities to be detected in patients with DS. Additionally, impaired GABAergic neurotransmission due to mutations in $Na_v1.1$ in the primary site of the circadian clock, the suprachiasmatic nucleus of the hypothalamus is associated with defects in the circadian clock in children afflicted with DS[123].

As mentioned above, deficits in action potential firing caused by mutations in $Na_v1.1$ in various classes of GABAergic interneurons leads to an imbalance of excitatory glutamatergic neurotransmission over inhibitory GABAergic neurotransmission in the central nervous system. This is considered to be the primary cause of the epileptic phenotype observed in DS supported by the other co-morbidities like developmental disabilities, ataxia, and cognitive defects. Characterization of the N722D variant in $Na_v1.1$ and use of computational models to model the empirical evidence obtained gives us a bigger picture view of the role the mutation plays in disease origin and progression.

5.4. Therapeutics

The therapeutics currently available for the treatment of DS are insufficient to ameliorate the seizures and other characteristic co-morbidities observed. Current treatment focuses on the use of cocktails of anti-epileptic drugs (AEDs) like valproate, clobazam, topiramate, and stiripentol to manage seizure activity[68,124] and prevent co-morbidities. The problem with using standard AEDs like lamotrigine for the treatment of DS lies in the mechanism of action of these pharmacological compounds. AEDs that are sodium channel blockers, work by reducing peak sodium currents, which have been found to exacerbate seizures in DS patients[125,126]. While classical AEDs might not be suitable, there have been studies showing use of atypical sodium channel blockers such as the GS967 could potentially be better suited to patients with DS[127]. Long term use of GS967 was associated with the inhibition of spontaneous action potential firing of pyramidal neurons. Removing the compound from neurons showed normalization of both sodium current density and voltage-dependence of activation. Parallelly, interneurons from chronically GS967-treated mice exhibited higher peak sodium current density which could serve as a rescue of loss-of function observed in $Na_v1.1$ N722D[128].

Another potential therapeutic could involve the use of $Na_v1.1$ specific activator compound, a 2- methylbenzamide derivative 3a. In a preliminary study, compound 3a has been shown to increase neuronal excitability by specifically lowering the threshold potentials to more negative values in fast-spiking inhibitory interneurons. As reported, compound 3a was able to increase the number of evoked action potentials even though the effect was most prominent after weak depolarizations that render a larger window available for further activity increase[129]. Further research needs to be done on optimizing the use dependent concentrations of this small molecule activator before it can be proposed as a potential therapeutic.

In DS, the primary effect of mutations in $Na_v1.1$ is the failure to generate action potentials in inhibitory GABAergic interneurons. Ideally, increasing the availability of GABA in the synaptic cleft while also increasing its postsynaptic effects would be one way to restore functioning in these mutated neurons. An inhibitor of the GAT1 transporter, Tiagabine inhibits the uptake of GABA from the synaptic cleft[130,131]. Subsequently, the benzodiazepine Clonazepam serves as an allosteric modulator to enhance the post synaptic response to GABA[132]. Due to the complementary molecular

mechanisms of enhancing GABAergic neurotransmission, studies have shown that combined therapy with Clonazepam and Tiagabine is additive, potentially increasing efficacy in prevention of seizures and reducing toxicity in patients with DS[133]. Together, the combination of these drugs might be able to reverse the disinhibition caused by impaired excitability of GABAergic interneurons leading to effective prevention of seizures with minimal adverse effects in patients with DS.

Various clinical trials in different phases of study are testing potential treatments for DS. The variable nature of causation underlying DS necessitates more creative approaches to the discovery of novel therapeutics. One such trial, sponsored by Stoke Therapeutics, is looking at an RNA based approach (STK001) using an anti-sense oligonucleotide to increase the level of healthy *SCN1A* messenger RNA in individuals with DS[134]. Another such study, ENDEAVOR, conducted by Encoded Therapeutics aims to use ETX101, a non-replicating, recombinant adeno-associated viral vector serotype 9 (rAAV9) to increase transcription levels of the *SCN1A* gene. Consisting of a GABAergic regulation element and an engineered transcription factor, ETX101 is intended to be used as a one-time intracerebroventricular therapeutic in young children with DS[135].

5.5. Limitations

In this study, the $Na_v1.1$ N722D mutation was characterized using a heterologous expression system. All experiments were performed in HEK293T cells, which cannot fully recapitulate the environment that is found in the native neuronal tissue in the central nervous system. There are many other interactive factors in neurons that modulate the functioning and expression properties of the channel in embryonic, neonatal, and mature adult stages. It might be beneficial to perform this study in different classes of native GABAergic inhibitory neurons to best mimic the channel functioning in its natural environment. However, there are drawbacks to the use of this system as well. To be able to accurately detect sodium specific current through the voltage-gated sodium channel, other non-specific ion channel currents in the tissue will have to be blocked using drugs and the effect of these drugs will have to be considered while interpreting results.

Sodium channels are a family of large molecular weight proteins (250 kDa). Using SDS-PAGE to resolve the proteins from whole-cell lysate in order to check for differences in molecular weights due to post-translational modifications proved to be very hard to do without using specialized kits. Due to their large band size and lack of resolution even when 8% gels were run, it was hard to ascertain if there were any differences in the final band sizes in the mutant bands when compared to the WT. Since sodium channels are highly glycosylated proteins, any differences in post-translational modifications that could be caused by the mutation would result in altered trafficking and expression properties of the channel. This could not be visualized when regular SDS-PAGE gels were run. In addition, due to the lack of availability of a phosphorylated $Na_v1.1$ Ab, I couldn't detect phosphorylation levels of the channels. Phosphorylation is another marker of post-translational modifications that would affect the channel trafficking properties to the plasma membrane of the cells. Specialized commercial kits to detect post translational modification effects are both expensive and require further processing steps that were out of the scope of this study.

Due to the highly flexible nature of the DI-DII linker region, the cryo-EM structure of $Na_v1.1$ that is currently available does not have the entire structure of this region resolved[64]. Therefore, it is hard to predict exactly what effect the mutation has on the channel configuration and structure. Until a fully characterized structure is resolved, any

predictions made about the interactions of $Na_v1.1$ N722D with other modulatory agents will contain some margin of error.

Chapter 6. Future Directions

This study was performed at room temperature (i.e. 22°C). It would be interesting to test the biophysical and expression characteristics of the channel at more physiological temperatures (37°C). Upon using more relevant physiological models, we might be able to see a more temperature dependent shift in the activation and inactivation properties of $Na_v1.1$ when compared to the data at 22°C. A recent study performed using a patient derived induced pluripotent stem cell model of Dravet Syndrome suggested novel mechanisms of action[136]. The study is proof that patient specific pathogenic neuronal ion channelopathies can be modeled using iPSC derived neurons. Not only is it helpful to study detailed pathogenesis, but it can also be used to find patient specific therapeutic pharmacological agents that work for each novel disease mechanism. If the same was done for $Na_v1.1$ N722D, we might be able to gain new insights into the mode of action of this particular mutant from early stages of disease progression.

There are over 150 mutations in the DI-DII linker region in $Na_v1.1$, many of which haven't been characterized yet[71]. Using a combination of computational models along with the biophysical characterization for all such mutations will help us gain a better understanding of the disease-causing mechanism of different genotypes. Apparently divergent mutations could follow similar pathophysiology, even if they differ functionally. This could, in turn, help identify similarities and dependence of site of mutation on the phenotypic characteristics observed.

Chapter 7. Conclusion

The presence of conserved structure, function, and regulation of voltage-gated ion channels is critical for normally propagating action potentials within neurons in the central nervous system. A multitude of factors, such as channel mutations, pharmacological treatments, pH, or temperature, may impair channel properties, leading to pathophysiological conditions like Dravet Syndrome. The missense mutation N722D in $Na_v1.1$ predisposes the patient to Dravet Syndrome. The vital underlying mechanism is a reduction of sodium current caused by a trafficking defect of mutant $Na_v1.1$ preventing its movement from the ER to the axolemma of the neuron. Achieving clinical improvements using information gathered from investigations into the biophysical properties of the channel alone will not be possible, especially in mutations like this where detailed study needs to be conducted into the various factors that could be causing the observed phenotype. When combined with computational modelling, neurophysiological studies could yield a treasure trove of information relating to the abnormal neuronal dynamics in patients. This information could then be used to formulate a personalized therapeutic plan for the patient that caters to their specific needs and addresses the root cause of the disease phenotype observed.

Chapter 8. References

1. Galvani: Opere scelte: a cura di Gustavo Barbensi - Google Scholar. https://scholar.google.com/scholar_lookup?title=Opere+scelte&publication_year=1967&author=L.+Galvani&inst=10441630620217902552.

2. Piccolino, M. Luigi Galvani's path to animal electricity. *C. R. Biol.* **329**, 303–318 (2006).

3. Hodgkin, A. L. & Huxley, A. F. Currents carried by sodium and potassium ions through the membrane of the giant axon of Loligo. *J. Physiol.* **116**, 449–472 (1952).

4. Hodgkin, A. L. & Huxley, A. F. A quantitative description of membrane current and its application to conduction and excitation in nerve. *J. Physiol.* **117**, 500–544 (1952).

5. Hodgkin, A. L. & Huxley, A. F. The dual effect of membrane potential on sodium conductance in the giant axon of Loligo. *J. Physiol.* **116**, 497–506 (1952).

6. Hodgkin, A. L. & Huxley, A. F. The components of membrane conductance in the giant axon of Loligo. *J. Physiol.* **116**, 473–496 (1952).

7. Catterall, W. A. & Beress, L. Sea anemone toxin and scorpion toxin share a common receptor site associated with the action potential sodium ionophore. *J. Biol. Chem.* **253**, 7393–7396 (1978).

8. Catterall, W. A. Neurotoxins that Act on Voltage-Sensitive Sodium Channels in Excitable Membranes. *http://dx.doi.org/10.1146/annurev.pa.20.040180.000311* **20**, 15–43 (2003).

9. Catterall, W. A. Binding of scorpion toxin to receptor sites associated with sodium channels in frog muscle: Correlation of voltage-dependent binding with activation. *J. Gen. Physiol.* **74**, 375–391 (1979).

10. Beneski, D. A. & Catterall, W. A. Covalent labeling of protein components of the sodium channel with a photoactivable derivative of scorpion toxin. *Proc. Natl. Acad. Sci.* **77**, 639–643 (1980).

11. Catterall, W. A. From ionic currents to molecular mechanisms: the structure and function of voltage-gated sodium channels. *Neuron* **26**, 13–25 (2000).

12. Isom, L. L. Sodium channel β subunits: Anything but auxiliary. *Neuroscientist* **7**, 42–54 (2001).

13. Chahine, M. & O'Leary, M. E. Regulatory Role of Voltage-Gated Na+ Channel β Subunits in Sensory Neurons. *Front. Pharmacol.* **2**, (2011).

14. Zhang, M. M. *et al.* Co-expression of NaVβ subunits alters the kinetics of inhibition of voltage-gated sodium channels by pore-blocking μ-conotoxins. *Br. J. Pharmacol.* **168**, 1597–1610 (2013).

15. Hartshorne, R. P. & Catterall, W. A. The sodium channel from rat brain. Purification and subunit composition. *J. Biol. Chem.* **259**, 1667–1675 (1984).

16. Noda, M. *et al.* Primary structure of Electrophorus electricus sodium channel deduced from cDNA sequence. *Nat. 1984 3125990* **312**, 121–127 (1984).

17. Heinemann, S. H., Terlau, H., Stühmer, W., Imoto, K. & Numa, S. Calcium channel characteristics conferred on the sodium channel by single mutations. *Nature* **356**, 441–443 (1992).

18. Catterall, W. A., Goldin, A. L. & Waxman, S. G. International Union of Pharmacology. XLVII. Nomenclature and structure-function relationships of voltage-gated sodium channels. *Pharmacol. Rev.* **57**, 397–409 (2005).

19. Noda, M., Suzuki, H., Numa, S. & Stühmer, W. A single point mutation confers tetrodotoxin and saxitoxin insensitivity on the sodium channel II. *FEBS Lett.* **259**, 213–216 (1989).

20. Scheuer, T. Regulation of Sodium Channel Activity by Phosphorylation. *Semin. Cell Dev. Biol.* **22**, 160 (2011).

21. Berendt, F. J., Park, K. S. & Trimmer, J. S. Multi-site Phosphorylation of Voltage-Gated Sodium Channel α Subunits from Rat Brain. *J. Proteome Res.* **9**, 1976 (2010).

22. Armstrong, C. M., Bezanilla, F. & Rojas, E. Destruction of Sodium Conductance Inactivation in Squid Axons Perfused with Pronase. *J. Gen. Physiol.* **62**, 375 (1973).

23. Hille: Ion channels of excitable membranes (Vol. 507) - Google Scholar. https://scholar.google.com/scholar?hl=en&as_sdt=0%2C5&cluster=4006670498233575323&inst=10441630620217902552.

24. Armstrong, C. M. Na channel inactivation from open and closed states. *Proc. Natl. Acad. Sci. U. S. A.* **103**, 17991–17996 (2006).

25. Bähring, R. & Covarrubias, M. Mechanisms of closed-state inactivation in voltage-gated ion channels. *J. Physiol.* **589**, 461–479 (2011).

26. Armstrong, C. M. & Bezanilla, F. Inactivation of the sodium channel. II. Gating current experiments. *J. Gen. Physiol.* **70**, 567 (1977).

27. Israel, M. R., Tay, B., Deuis, J. R. & Vetter, I. Sodium Channels and Venom Peptide Pharmacology. *Adv. Pharmacol.* **79**, 67–116 (2017).

28. Goldin, A. L. Diversity of Mammalian Voltage-Gated Sodium Channels. *Ann. N. Y. Acad. Sci.* **868**, 38–50 (1999).

29. Watanabe, E. *et al.* Nav2/NaG channel is involved in control of salt-intake behavior in the CNS. *J. Neurosci.* **20**, 7743–7751 (2000).

30. De Lera Ruiz, M. & Kraus, R. L. Voltage-Gated Sodium Channels: Structure, Function, Pharmacology, and Clinical Indications. *J. Med. Chem.* **58**, 7093–7118 (2015).

31. Shao, D., Okuse, K. & Djamgoz, M. B. A. Protein-protein interactions involving voltage-gated sodium channels: Post-translational regulation, intracellular trafficking and functional expression. *Int. J. Biochem. Cell Biol.* **41**, 1471–1481 (2009).

32. Meisler, M. H. & Kearney, J. A. Sodium channel mutations in epilepsy and other neurological disorders. *J. Clin. Invest.* **115**, 2010 (2005).

33. Van Wart, A., Trimmer, J. S. & Matthews, G. Polarized Distribution of Ion Channels within Microdomains of the Axon Initial Segment. (2006) doi:10.1002/cne.21173.

34. Cheah, C. S. *et al.* Specific deletion of NaV1.1 sodium channels in inhibitory interneurons causes seizures and premature death in a mouse model of Dravet syndrome. *Proc. Natl. Acad. Sci. U. S. A.* **109**, 14646–14651 (2012).

35. Claes, L. *et al.* De Novo Mutations in the Sodium-Channel Gene SCN1A Cause Severe Myoclonic Epilepsy of Infancy. *Am. J. Hum. Genet.* **68**, 1327–1332 (2001).

36. Escayg, A. *et al.* Mutations of SCN1A, encoding a neuronal sodium channel, in two families with GEFS+2. *Nat. Genet.* **24**, 343–345 (2000).

37. Mantegazza, M. *et al.* Identification of an Nav1.1 sodium channel (SCN1A) loss-of-function mutation associated with familial simple febrile seizures. *Proc. Natl. Acad. Sci. U. S. A.* **102**, 18177–18182 (2005).

38. Nelson, K. B. & Ellenberg, J. H. Predictors of epilepsy in children who have experienced febrile seizures. *N. Engl. J. Med.* **295**, 1029–1033 (1976).

39. Generalized epilepsy with febrile seizures plus: A common childhood-onset genetic epilepsy syndrome - Singh - 1999 - Annals of Neurology - Wiley Online Library. https://onlinelibrary.wiley.com/doi/abs/10.1002/1531-8249%28199901%2945%3A1%3C75%3A%3AAID-ART13%3E3.0.CO%3B2-W?sid=nlm%3Apubmed.

40. Scheffer, I. E. & Berkovic, S. F. Generalized epilepsy with febrile seizures plus. A genetic disorder with heterogeneous clinical phenotypes. *Brain* **120 (Pt 3)**, 479–490 (1997).

41. Scheffer, I. E. & Berkovic, S. F. Generalized epilepsy with febrile seizures plus. A genetic disorder with heterogeneous clinical phenotypes. *Brain* **120**, 479–490 (1997).

42. Yu, F. H. *et al.* Reduced sodium current in GABAergic interneurons in a mouse model of severe myoclonic epilepsy in infancy. *Nat. Neurosci.* **9**, 1142–1149 (2006).

43. Yu, F. H. *et al.* Reduced sodium current in GABAergic interneurons in a mouse model of severe myoclonic epilepsy in infancy. *Nat. Neurosci. 2006 99* **9**, 1142–1149 (2006).

44. Kalume, F., Yu, F. H., Westenbroek, R. E., Scheuer, T. & Catterall, W. A. Reduced Sodium Current in Purkinje Neurons from NaV1.1 Mutant Mice: Implications for Ataxia in Severe Myoclonic Epilepsy in Infancy. *J. Neurosci.* **27**, 11065–11074 (2007).

45. Spampanato, J., Escayg, A., Meisler, M. H. & Goldin, A. L. Functional Effects of Two Voltage-Gated Sodium Channel Mutations That Cause Generalized Epilepsy with Febrile Seizures Plus Type 2. *J. Neurosci.* **21**, 7481 (2001).

46. Spampanato, J., Escayg, A., Meisler, M. H. & Goldin, A. L. Generalized epilepsy with febrile seizures plus type 2 mutation W1204R alters voltage-dependent gating of Nav1.1 sodium channels. *Neuroscience* **116**, 37–48 (2003).

47. Spampanato, J. *et al.* A Novel Epilepsy Mutation in the Sodium Channel SCN1A Identifies a Cytoplasmic Domain for β Subunit Interaction. *J. Neurosci.* **24**, 10022 (2004).

48. Barela, A. J. *et al.* An Epilepsy Mutation in the Sodium Channel SCN1A ThatDecreases Channel Excitability. *J. Neurosci.* **26**, 2714 (2006).

49. Alekov, A. K., Rahman, M. M., Mitrovic, N., Lehmannhorn, F. & Lerche, H. A sodium channel mutation causing epilepsy in man exhibits subtle defects in fast inactivation and activation in vitro. *J. Physiol.* **529**, 533 (2000).

50. Alekov, A. K., Masmudur Rahman, M. D., Mitrovic, N., Lehmann-Horn, F. & Lerche, H. Enhanced inactivation and acceleration of activation of the sodium channel associated with epilepsy in man. *Eur. J. Neurosci.* **13**, 2171–2176 (2001).

51. Peters, C., Rosch, R. E., Hughes, E. & Ruben, P. C. Temperature-dependent changes in neuronal dynamics in a patient with an SCN1A mutation and hyperthermia induced seizures. *Sci. Rep.* **6**, (2016).

52. Rhodes, T. H., Lossin, C., Vanoye, C. G., Wang, D. W. & George, A. L. Noninactivating voltage-gated sodium channels in severe myoclonic epilepsy of infancy. *Proc. Natl. Acad. Sci. U. S. A.* **101**, 11147 (2004).

53. Lossin, C. *et al.* Epilepsy-Associated Dysfunction in the Voltage-Gated Neuronal Sodium Channel SCN1A. *J. Neurosci.* **23**, 11289 (2003).

54. Thompson, C. H., Porter, J. C., Kahlig, K. M., Daniels, M. A. & George, A. L. Nontruncating SCN1A Mutations Associated with Severe Myoclonic Epilepsy of Infancy Impair Cell Surface Expression. *J. Biol. Chem.* **287**, 42001–42008 (2012).

55. Shao, D., Okuse, K. & Djamgoz, M. B. A. Protein–protein interactions involving voltage-gated sodium channels: Post-translational regulation, intracellular trafficking and functional expression. *Int. J. Biochem. Cell Biol.* **41**, 1471–1481 (2009).

56. Rusconi, R. *et al.* Modulatory Proteins Can Rescue a Trafficking Defective Epileptogenic Nav1.1 Na+ Channel Mutant. *J. Neurosci.* **27**, 11037 (2007).

57. Cantrell, A. R., Smith, R. D., Goldin, A. L., Scheuer, T. & Catterall, W. A. Dopaminergic modulation of sodium current in hippocampal neurons via cAMP-dependent phosphorylation of specific sites in the sodium channel alpha subunit. *J. Neurosci.* **17**, 7330–7338 (1997).

58. Annesi, G. *et al.* Two Novel SCN1A Missense Mutations in Generalized Epilepsy with Febrile Seizures Plus. *Epilepsia* **44**, 1257–1258 (2003).

59. Barela, A. J. *et al.* An Epilepsy Mutation in the Sodium Channel SCN1A ThatDecreases Channel Excitability. *J. Neurosci.* **26**, 2714 (2006).

60. Escayg, A. *et al.* A Novel SCN1A Mutation Associated with Generalized Epilepsy with Febrile Seizures Plus—and Prevalence of Variants in Patients with Epilepsy. *Am. J. Hum. Genet.* **68**, 866 (2001).

61. Osaka, H. *et al.* Patients with a sodium channel alpha 1 gene mutation show wide phenotypic variation. *Epilepsy Res.* **75**, 46–51 (2007).

62. Depienne, C. *et al.* Spectrum of SCN1A gene mutations associated with Dravet syndrome: analysis of 333 patients. *J. Med. Genet.* **46**, 183–191 (2009).

63. Bechi, G. *et al.* Rescuable folding defective NaV1.1 (SCN1A) mutants in epilepsy: Properties, occurrence, and novel rescuing strategy with peptides targeted to the endoplasmic reticulum. *Neurobiol. Dis.* **75**, 100–114 (2015).

64. Pan, X. *et al.* Comparative structural analysis of human Nav1.1 and Nav1.5 reveals mutational hotspots for sodium channelopathies. *Proc. Natl. Acad. Sci.* **118**, (2021).

65. org, W. D. pymol. & 2002, undefined. The PyMOL molecular graphics system. *ci.nii.ac.jp*.

66. Catterall, W. A. Dravet Syndrome: A Sodium Channel Interneuronopathy. *Curr. Opin. Physiol.* **2**, 42 (2018).

67. Dravet, C. The core Dravet syndrome phenotype. *Epilepsia* **52 Suppl 2**, 3–9 (2011).

68. Chiron, C. & Dulac, O. The pharmacologic treatment of Dravet syndrome. *Epilepsia* **52 Suppl 2**, 72–75 (2011).

69. Catterall, W. A., Kalume, F. & Oakley, J. C. NaV1.1 channels and epilepsy. *J. Physiol.* **588**, 1849 (2010).

70. George, A. L. Inherited disorders of voltage-gated sodium channels. *J. Clin. Invest.* **115**, 1990–1999 (2005).

71. Meng, H. *et al.* The SCN1A Mutation Database: Updating Information and Analysis of the Relationships among Genotype, Functional Alteration, and Phenotype. *Off. J. Hum Mutat* **36**, 573–580 (2015).

72. Tai, C., Abe, Y., Westenbroek, R. E., Scheuer, T. & Catterall, W. A. Impaired excitability of somatostatin- and parvalbumin-expressing cortical interneurons in a mouse model of Dravet syndrome. *Proc. Natl. Acad. Sci. U. S. A.* **111**, E3139 (2014).

73. Oakley, J. C., Kalume, F. & Catterall, W. A. Insights into pathophysiology and therapy from a mouse model of Dravet syndrome. *Epilepsia* **52 Suppl 2**, 59–61 (2011).

74. Dylke, J., Lopes, J., Dang-Lawson, M., Machtaler, S. & Matsuuchi, L. Role of the extracellular and transmembrane domain of Ig-alpha/beta in assembly of the B cell antigen receptor (BCR). *Immunol. Lett.* **112**, 47–57 (2007).

75. Lossin, C. A catalog of SCN1A variants. *Brain Dev.* **31**, 114–130 (2009).

76. Escayg, A. & Goldin, A. L. Sodium channel SCN1A and epilepsy: mutations and mechanisms. *Epilepsia* **51**, 1650 (2010).

77. Claes, L. R. F. *et al.* The SCN1A variant database: a novel research and diagnostic tool. *Hum. Mutat.* **30**, E904–E920 (2009).

78. Zuberi, S. M. *et al.* Genotype-phenotype associations in SCN1A-related epilepsies. *Neurology* **76**, 594–600 (2011).

79. Ohmori, I., Kahlig, K. M., Rhodes, T. H., Wang, D. W. & George, A. L. Nonfunctional SCN1A is common in severe myoclonic epilepsy of infancy. *Epilepsia* **47**, 1636–1642 (2006).

80. Sugawara, T. *et al.* Frequent mutations of SCN1A in severe myoclonic epilepsy in infancy. *Neurology* **58**, 1122–1124 (2002).

81. Arribas-Blázquez, M. *et al.* Regulation of the voltage-dependent sodium channel NaV1.1 by AKT1. *Neuropharmacology* **197**, 108745 (2021).

82. Galleano, I. *et al.* Functional cross-talk between phosphorylation and disease-causing mutations in the cardiac sodium channel Nav1.5. *Proc. Natl. Acad. Sci. U. S. A.* **118**, e2025320118 (2021).

83. Sanders, C. R. & Myers, J. K. Disease-Related Misassembly of Membrane Proteins. *https://doi.org/10.1146/annurev.biophys.33.110502.140348* **33**, 25–51 (2004).

84. Allouis, M. *et al.* 14-3-3 is a regulator of the cardiac voltage-gated sodium channel Nav1.5. *Circ. Res.* **98**, 1538–1546 (2006).

85. Boyle, L. H., Gillingham, A. K., Munro, S. & Trowsdale, J. Selective Export of HLA-F by Its Cytoplasmic Tail. *J. Immunol.* **176**, 6464–6472 (2006).

86. Carr, D. B. *et al.* Transmitter modulation of slow, activity-dependent alterations in sodium channel availability endows neurons with a novel form of cellular plasticity. *Neuron* **39**, 793–806 (2003).

87. Tibbs, V. C., Gray, P. C., Catterall, W. A. & Murphy, B. J. AKAP15 anchors cAMP-dependent protein kinase to brain sodium channels. *J. Biol. Chem.* **273**, 25783–25788 (1998).

88. Zhou, Z., Gong, Q. & January, C. T. Correction of defective protein trafficking of a mutant HERG potassium channel in human long QT syndrome. Pharmacological and temperature effects. *J. Biol. Chem.* **274**, 31123–31126 (1999).

89. Ficker, E., Obejero-Paz, C. A., Zhao, S. & Brown, A. M. The binding site for channel blockers that rescue misprocessed human long QT syndrome type 2 ether-a-gogo-related gene (HERG) mutations. *J. Biol. Chem.* **277**, 4989–4998 (2002).

90. Bernier, V., Lagacé, M., Bichet, D. G. & Bouvier, M. Pharmacological chaperones: Potential treatment for conformational diseases. *Trends Endocrinol. Metab.* **15**, 222–228 (2004).

91. Kearney, J. A. Double Trouble: Impairment of Two Interneuron Types in a Dravet Mouse Model. *Epilepsy Curr.* **15**, 47 (2015).

92. CJ, M. & A, F. Interneurons unbound. *Nat. Rev. Neurosci.* **2**, 11–23 (2001).

93. Pouille, F. & Scanziani, M. Enforcement of temporal fidelity in pyramidal cells by somatic feed-forward inhibition. *Science* **293**, 1159–1163 (2001).

94. Wehr, M. & Zador, A. M. Balanced inhibition underlies tuning and sharpens spike timing in auditory cortex. *Nature* **426**, 442–446 (2003).

95. Markram, H. *et al.* Interneurons of the neocortical inhibitory system. *Nature Reviews Neuroscience* vol. 5 793–807 (2004).

96. Trevelyan, A. J., Sussillo, D., Watson, B. O. & Yuste, R. Modular Propagation of Epileptiform Activity: Evidence for an Inhibitory Veto in Neocortex. *J. Neurosci.* **26**, 12447 (2006).

97. Klausberger, T. & Somogyi, P. Neuronal Diversity and Temporal Dynamics: The Unity of Hippocampal Circuit Operations. *Science* **321**, 53 (2008).

98. Haider, B. & McCormick, D. A. Rapid Neocortical Dynamics: Cellular and Network Mechanisms. *Neuron* **62**, 171 (2009).

99. Noebels, J. L. The biology of epilepsy genes. *Annu. Rev. Neurosci.* **26**, 599–625 (2003).

100. Cobos, I. *et al.* Mice lacking Dlx1 show subtype-specific loss of interneurons, reduced inhibition and epilepsy. *Nat. Neurosci.* **8**, 1059–1068 (2005).

101. Gonzalez-Burgos, G. & Lewis, D. A. GABA Neurons and the Mechanisms of Network Oscillations: Implications for Understanding Cortical Dysfunction in Schizophrenia. *Schizophr. Bull.* **34**, 944 (2008).

102. Cossart, R. *et al.* Dendritic but not somatic GABAergic inhibition is decreased in experimental epilepsy. *Nat. Neurosci.* **4**, 52–62 (2001).

103. Levitt, P., Eagleson, K. L. & Powell, E. M. Regulation of neocortical interneuron development and the implications for neurodevelopmental disorders. *Trends Neurosci.* **27**, 400–406 (2004).

104. Pouille, F., Marin-Burgin, A., Adesnik, H., Atallah, B. V. & Scanziani, M. Input normalization by global feedforward inhibition expands cortical dynamic range. *Nat. Neurosci.* **12**, 1577–1585 (2009).

105. Zemankovics, R., Veres, J. M., Oren, I. & Hájos, N. Feedforward inhibition underlies the propagation of cholinergically induced gamma oscillations from hippocampal CA3 to CA1. *J. Neurosci.* **33**, 12337–12351 (2013).

106. Traub, R. D. *et al.* GABA-enhanced collective behavior in neuronal axons underlies persistent gamma-frequency oscillations. *Proc. Natl. Acad. Sci. U. S. A.* **100**, 11047 (2003).

107. Rossignol, E. Genetics and Function of Neocortical GABAergic Interneurons in Neurodevelopmental Disorders. *Neural Plast.* **2011**, 25 (2011).

108. Bartos, M., Vida, I. & Jonas, P. Synaptic mechanisms of synchronized gamma oscillations in inhibitory interneuron networks. *Nat. Rev. Neurosci.* **8**, 45–56 (2007).

109. Cardin, J. A. *et al.* Driving fast-spiking cells induces gamma rhythm and controls sensory responses. *Nature* **459**, 663 (2009).

110. Tallon-Baudry, C., Bertrand, O., Peronnet, F. & Pernier, J. Induced γ-Band Activity during the Delay of a Visual Short-Term Memory Task in Humans. *J. Neurosci.* **18**, 4244 (1998).

111. Sohal, V. S., Zhang, F., Yizhar, O. & Deisseroth, K. Parvalbumin neurons and gamma rhythms enhance cortical circuit performance. *Nature* **459**, 698 (2009).

112. Lewis, D. A., Hashimoto, T. & Volk, D. W. Cortical inhibitory neurons and schizophrenia. *Nat. Rev. Neurosci.* **6**, 312–324 (2005).

113. Spencer, K. M. *et al.* Abnormal Neural Synchrony in Schizophrenia. *J. Neurosci.* **23**, 7407 (2003).

114. Spencer, K. M. *et al.* Neural synchrony indexes disordered perception and cognition in schizophrenia. *Proc. Natl. Acad. Sci. U. S. A.* **101**, 17288 (2004).

115. Cho, R. Y., Konecky, R. O. & Carter, C. S. Impairments in frontal cortical γ synchrony and cognitive control in schizophrenia. *Proc. Natl. Acad. Sci. U. S. A.* **103**, 19878 (2006).

116. Berger, T. K., Perin, R., Silberberg, G. & Markram, H. Frequency-dependent disynaptic inhibition in the pyramidal network: a ubiquitous pathway in the developing rat neocortex. *J. Physiol.* **587**, 5411 (2009).

117. Silberberg, G. & Markram, H. Disynaptic inhibition between neocortical pyramidal cells mediated by Martinotti cells. *Neuron* **53**, 735–746 (2007).

118. Glickfeld, L. L., Roberts, J. D., Somogyi, P. & Scanziani, M. Interneurons hyperpolarize pyramidal cells along their entire somatodendritic axis. *Nat. Neurosci.* **12**, 21 (2009).

119. Powell, E. M. *et al.* Genetic Disruption of Cortical Interneuron Development Causes Region- and GABA Cell Type-Specific Deficits, Epilepsy, and Behavioral Dysfunction. *J. Neurosci.* **23**, 622 (2003).

120. Powell, E. M., Mars, W. M. & Levitt, P. Hepatocyte growth factor/scatter factor is a motogen for interneurons migrating from the ventral to dorsal telencephalon. *Neuron* **30**, 79–89 (2001).

121. Bae, M. H. *et al.* Hepatocyte growth factor (HGF) modulates GABAergic inhibition and seizure susceptibility. *Exp. Neurol.* **221**, 129 (2010).

122. Kalume, F., Yu, F. H., Westenbroek, R. E., Scheuer, T. & Catterall, W. A. Reduced Sodium Current in Purkinje Neurons from NaV1.1 Mutant Mice: Implications for Ataxia in Severe Myoclonic Epilepsy in Infancy. *J. Neurosci.* **27**, 11065 (2007).

123. Nolan, K., Camfield, C. S. & Camfield, P. R. Coping with a child with Dravet syndrome: insights from families. *J. Child Neurol.* **23**, 690–694 (2008).

124. Volkers, L. *et al.* Nav1.1 Dysfunction in Genetic Epilepsy with Febrile Seizures Plus or Dravet Syndrome. *Eur. J. Neurosci.* **34**, 1268 (2011).

125. Guerrini, R. *et al.* Lamotrigine and seizure aggravation in severe myoclonic epilepsy. *Epilepsia* **39**, 508–512 (1998).

126. Hawkins, N. A. *et al.* Screening of conventional anticonvulsants in a genetic mouse model of epilepsy. *Ann. Clin. Transl. Neurol.* **4**, 326 (2017).

127. Koltun, D. O. *et al.* Discovery of triazolopyridine GS-458967, a late sodium current inhibitor (Late INai) of the cardiac NaV 1.5 channel with improved efficacy and potency relative to ranolazine. *Bioorg. Med. Chem. Lett.* **26**, 3202–3206 (2016).

128. Anderson, L. L., Hawkins, N. A., Thompson, C. H., Kearney, J. A. & George, A. L. Unexpected Efficacy of a Novel Sodium Channel Modulator in Dravet Syndrome. *Sci. Rep.* **7**, (2017).

129. Crestey, F. *et al.* Identification and Electrophysiological Evaluation of 2-Methylbenzamide Derivatives as Nav1.1 Modulators. *ACS Chem. Neurosci.* **6**, 1302–1308 (2015).

130. Meldrum, B. S. & Chapman, A. G. Basic mechanisms of gabitril (tiagabine) and future potential developments. *Epilepsia* **40 Suppl 9**, (1999).

131. Bauer, J. & Cooper-Mahkorn, D. Tiagabine: efficacy and safety in partial seizures – current status. *Neuropsychiatr. Dis. Treat.* **4**, 731 (2008).

132. Rudolph, U. & Möhler, H. Analysis of GABAA receptor function and dissection of the pharmacology of benzodiazepines and general anesthetics through mouse genetics. *Annu. Rev. Pharmacol. Toxicol.* **44**, 475–498 (2004).

133. Oakley, J. C., Cho, A. R., Cheah, C. S., Scheuer, T. & Catterall, W. A. Synergistic GABA-Enhancing Therapy against Seizures in a Mouse Model of Dravet Syndrome. *J. Pharmacol. Exp. Ther.* **345**, 215 (2013).

134. An Open-Label Extension Study of STK-001 for Patients With Dravet Syndrome - Full Text View - ClinicalTrials.gov. https://clinicaltrials.gov/ct2/show/study/NCT04740476?term=Dravet+Syndrome&draw=2&rank=3.

135. A Clinical Study to Evaluate the Safety and Efficacy of ETX101 in Infants and Children With SCN1A-Positive Dravet Syndrome - Full Text View - ClinicalTrials.gov. https://clinicaltrials.gov/ct2/show/NCT05419492?term=Dravet+Syndrome&draw=2&rank=6.

136. Liu, Y. *et al.* Dravet syndrome patient-derived neurons suggest a novel epilepsy mechanism. *Ann. Neurol.* **74**, 128–139 (2013).